

UNCLASSIFIED

Copy 46
RM-A50L07
RM A50L07 c.1

NACA RM A50L07

NACA
CASE FILE
COPY
RESEARCH MEMORANDUM

UNCLASSIFIED

Authority

DOD DIR 5200.10

Date 11/5/64 By S Jackson

CHARACTERISTICS OF FLOW OVER INCLINED

BODIES OF REVOLUTION

By H. Julian Allen and Edward W. Perkins

Ames Aeronautical Laboratory
Moffett Field, Calif.

CLASSIFIED DOCUMENT

This document contains classified information affecting the National Defense of the United States within the meaning of the Espionage Act, USC 50:31 and 32. Its transmission or the revelation of its contents in any manner to an unauthorized person is prohibited by law.

Information so classified may be imparted only to persons in the military and naval services of the United States, appropriate civilian officers and employees of the Federal Government who have a legitimate interest therein, and to United States citizens of known loyalty and discretion who of necessity must be informed thereof.

GROUP 4

Downgraded at 3 year

intervals; declassified

or 12 years

**NATIONAL ADVISORY COMMITTEE
FOR AERONAUTICS**

WASHINGTON

March 5, 1951

UNCLASSIFIED

MAR 13 1951

NATIONAL ADVISORY COMMITTEE FOR AERONAUTICS

RESEARCH MEMORANDUMCHARACTERISTICS OF FLOW OVER INCLINED
BODIES OF REVOLUTION

By H. Julian Allen and Edward W. Perkins

SUMMARY

Experimental force, moment, and center-of-pressure variations for a large number of bodies of revolution have been compared with the calculated characteristics based on the approximate theory developed in NACA RM A9I26. The bodies varied in fineness ratio from 4.5 to 21.1, from blunt unboattailed bodies to airship hulls, and the experimental results are given for widely varying Mach numbers and ranges of angle of attack. It is shown that the lift and drag characteristics are fairly accurately predicted by the theory but that the actual center of pressure is more rearward than the theory indicates.

Experimental pressure distributions and visual-flow studies which have been used to investigate the characteristics of the cross flow for inclined bodies of revolution have demonstrated that the development of the cross flow with distance along the body on a long body of constant diameter behaves much the same as the development with time of the flow about a circular cylinder impulsively started from rest. This fact assists in explaining the observed differences between center-of-pressure location determined from experiment and that calculated using the approximate theory.

INTRODUCTION

There has long been considerable interest in the forces and moments experienced by bodies of revolution in inclined flight. The original interest pertained to the forces and moments on airship hulls. Max Munk (reference 1) considered the potential flow about such hull shapes and showed that at any station along a hull at angle of attack α a local force per unit length of magnitude

$$(k_2 - k_1) q \frac{ds}{dx} \sin 2\alpha$$

[REDACTED]

should be experienced. (See appendix A for symbols.) From the later work of G. N. Ward (reference 2) it may be shown that this force is directed midway between the normal to the axis of revolution and the normal to the wind direction.

These potential flow theories predict that for any closed body, such as an airship hull, at angle of attack a pitching moment but no net cross force should be experienced. A comparison between calculated and experimental moments about the centers of volume on airship hulls showed that the moments experienced were always less than those calculated (usually of the order of 70 or 80 percent of the theoretical values). Contrary to theory, experiment showed that, in fact, a cross force did occur which was small at small angles of attack but increased rapidly with increasing angle of inclination, the cross force always being directed toward the lee side of the body. Experiment also showed an increase in drag with angle of attack which was not indicated by theory. It has long been recognized that the discrepancies between this potential theory and experiment resulted from the failure to consider the action of viscosity in the theoretical treatment. The results of a detailed experimental study of the flow field about an airship model in inclined flow, which was made by R. P. Harrington (reference 3), clearly demonstrated the importance of these viscous effects.

In recent times, a primary interest in the body-of-revolution problem has arisen for missiles and supersonic aircraft where the body again becomes a major component of the configurations. These bodies are, in general, slender, blunt-based bodies for which H. S. Tsien (reference 4) has shown the potential theory still to be applicable at small angles of attack even at supersonic speeds. For these blunt-based bodies the potential theory indicates that a net cross force, a pitching moment, and a drag increment will occur in inclined flow. However, from available experimental data, it is apparent that, in general, while the moment about the center of volume is less than would be calculated from potential theory, the net cross force and the drag increment are larger than calculated, the discrepancy becoming increasingly apparent with increasing angle of inclination.

R. T. Jones (reference 5) showed theoretically that on an infinitely long inclined cylinder with laminar-boundary-layer flow, the viscous flow across the cylinder may be treated independently of the flow along the cylinder. Thus the component of flow across such an inclined cylinder would be expected to behave the same as the two-dimensional flow across the cylinder at a velocity equal to the product of the flow velocity past the inclined cylinder and the sine of the angle of inclination. Accordingly, in reference 6, it was postulated that a better evaluation of the cross-force distribution on a body of revolution of finite length (see fig. 1) moving at the velocity V_0 could be obtained by adding to the potential cross-force distribution an additional cross

[REDACTED]

force calculated on the assumption that each circular element along the hull experienced a force equal to the drag force which would be experienced by an element of a circular cylinder of the same diameter in a stream moving at the cross component of the stream velocity, $V_0 \sin \alpha$.¹ That is, the total cross force per unit length at any station could be given by an expression which is the sum of the potential cross force and a term to account for the viscous cross force. Thus

$$f = (k_2 - k_1) q \frac{ds}{dx} \sin 2\alpha \cos \frac{\alpha}{2} + 2\eta c_{dc} r q \sin^2 \alpha \quad (1)$$

With this simple allowance for viscous effects the lift coefficient,² the fore-drag coefficient, and the pitching moment coefficient about an arbitrary position a distance x_m from the nose are given by

$$\left. \begin{aligned} C_L &= (k_2 - k_1) \frac{S_b}{A} \sin 2\alpha \cos \frac{\alpha}{2} + \eta c_{dc} \left(\frac{A_p}{A} \right) \sin^2 \alpha \cos \alpha \\ C_{DF} &= C_{DF(\alpha=0)} \cos^3 \alpha + (k_2 - k_1) \frac{S_b}{A} \sin 2\alpha \sin \frac{\alpha}{2} + \eta c_{dc} \left(\frac{A_p}{A} \right) \sin^3 \alpha \\ C_M &= (k_2 - k_1) \left(\frac{vol - S_b (l - x_m)}{AX} \right) \sin 2\alpha \cos \frac{\alpha}{2} + \\ &\quad \eta c_{dc} \left(\frac{A_p}{A} \right) \left(\frac{x_m - x_p}{X} \right) \sin^2 \alpha \end{aligned} \right\} \quad (2)$$

Because of the approximate nature of the theory, it is not considered justified to retain the complex forms of these equations. Accordingly, it is assumed that for the functions of the angle of attack cosines may be replaced by unity and sines by the angles in radians to give³

¹A similar suggestion has also been made by Milton Van Dyke in a paper presented at the 1950 winter meeting of the Institute of Aeronautical Sciences.

²In the expression for C_L the contribution of the axial drag force $-C_{DF(\alpha=0)} \cos^2 \alpha \sin \alpha$ is inconsequentially small and has been ignored.

³In the expression for ΔC_{DF} the term $-C_{DF(\alpha=0)} \alpha^2$, which should properly appear on the right-hand side of this equation, has been omitted since for all practical cases its contribution to the drag increment is so small that it may be ignored.

$$\left. \begin{aligned}
 C_L &= 2(k_2 - k_1) \left(\frac{S_b}{A} \right) \alpha + \eta c_{dc} \left(\frac{A_p}{A} \right) \alpha^2 \\
 \Delta C_{DF} &= C_{DF} - C_{DF\alpha=0} = (k_2 - k_1) \left(\frac{S_b}{A} \right) \alpha^2 + \eta c_{dc} \left(\frac{A_p}{A} \right) \alpha^3 \\
 C_M &= 2(k_2 - k_1) \left(\frac{v_{g1} - S_b (1-x_m)}{AX} \right) \alpha + \eta c_{dc} \left(\frac{A_p}{A} \right) \left(\frac{x_m - x_p}{X} \right) \alpha^2
 \end{aligned} \right\} (3)$$

The first term on the right side of each of these equations is the potential contribution, while the second term is the viscous contribution.

Clearly, this suggested allowance for viscous effects is very approximate and could only be expected to apply well for bodies of very high fineness ratio by virtue of the assumed two-dimensional nature of the viscous cross flow. The remainder of this paper will be devoted, first, to a determination of the adequacy of this method for predicting the force and moment characteristics for a large number of bodies of practical fineness ratios and, second, to an investigation of the nature of the cross flow to ascertain wherein the actual development of the viscous cross forces differs from that assumed in the foregoing treatment. The latter study will provide a qualitative explanation of the observed differences between the calculated and experimental characteristics and to indicate that other important effects of viscosity must be taken into consideration.

COMPARISON OF CALCULATED AND EXPERIMENTAL FORCE AND MOMENT CHARACTERISTICS

In figures 2 to 11 are shown the experimental force, moment, and center-of-pressure characteristics as a function of angle of attack for a representative group of bodies of revolution from references 7 to 17 and from tests at the Ames Aeronautical Laboratory. The bodies vary in fineness ratio from 4.5 to 21.1, from blunt unboattailed bodies to airship hulls, and the experimental results are given for widely varying Mach numbers and ranges of angles of attack.

The dashed curves of figures 2 to 11 show the characteristics calculated by potential theory, while, unless otherwise indicated, the solid curves are based on equations (3). These latter expressions which include the allowance for the influence of viscosity will be referred to hereinafter as the viscous theory. The value of $k_2 - k_1$

was taken as unity except for the two airship hulls and for the 50-caliber shell.⁴ To calculate the force and moment characteristics by equations (3), it is necessary to evaluate the coefficients c_{dc} , the section drag coefficient of a circular cylinder, and η , the ratio of the drag coefficient of a circular cylinder of finite length to the drag coefficient of a circular cylinder of infinite length. The section-drag coefficients of circular cylinders have been determined for a wide range of Reynolds numbers and Mach numbers. (See references 18 to 23.) Experimental data from a number of sources have been plotted in figures 12 and 13 to show these variations. With regard to the evaluation of η , the only available experimental data (reference 24) have been plotted in figure 14 and a discussion of possible extensions of these data to Mach and Reynolds numbers other than those for which the data were obtained has been included in appendix B.

Effect of Cross-Flow Reynolds Number

There is a wide range of Reynolds numbers (see fig. 12) from about 10^4 to 2×10^5 for which, at low Mach numbers, the section-drag coefficient is constant and equal to 1.2. All the experimental data from figures 2 through 6 correspond to cross Reynolds numbers at low cross Mach numbers for which this value of cross drag coefficient is appropriate. Examination of these figures shows that the lift, fore-drag increment, and center-of-pressure position are much more adequately predicted by equations (3) than by the potential theory. The lift and fore-drag increment are seriously underestimated by potential theory at high angles of attack. Contrary to potential theory, the experimental center-of-pressure position varies with angle of attack. The variation is similar to that indicated by the viscous theory, but the actual center of pressure is farther toward the base of the body (generally by about one body diameter) than the viscous theory indicates. In the case of the pitching moments, the experimental values are, in all cases for which the center of moments is at or near the center of volume, smaller in absolute magnitude than the values calculated by either theory. (In the case of the body of fig. 3, the moment reference center was accidentally chosen so that the experimental values agree with the potential theory. Since the lift and center-of-pressure positions are so poorly

⁴Since an extensive dead-air region must exist in the wake of a blunt-based body, the effective length-diameter ratio determining the apparent mass coefficients must be greater than the actual. For all the blunt-based bodies except the 50-caliber shell, the actual fineness ratio was so large that a value of k_2-k_1 of unity was appropriate. For the relatively short shell model the effective fineness ratio was arbitrarily assumed to be twice the actual.

predicted by potential theory, it is apparent that the agreement between the experimental moment results and the moment variation predicted by potential theory must be accidental.)

It is well known that for Mach numbers below approximately 0.4 there is a critical Reynolds number range for a circular cylinder. Within this Reynolds number range the drag coefficient drops from 1.2 to approximately 0.3 with increasing Reynolds number. It was anticipated that for inclined bodies of revolution, since the cross Reynolds number increases with angle of attack, erratic variations of lift and moment with angle of attack might result if the cross Reynolds numbers fell in this critical range. A review of available literature revealed that data for two bodies of revolution were available wherein the cross Reynolds number based on the maximum diameter of the body exceeded the critical Reynolds number for a circular cylinder. These are the force-test results of the hull model of the airship Akron (reference 15) and of the RM-10 (reference 16). For the Akron, the experiments were conducted at several Reynolds numbers at negligibly low Mach numbers. Figure 7 shows for the minimum and maximum test Reynolds numbers the forces, moments, and centers of pressure calculated for the Akron from equations (3) using the appropriate values of c_{dc} from figure 12. These curves indicate an erratic variation of the parameters with angle of attack, being different for the two Reynolds numbers. However, the experimental values are seen to be independent of the Reynolds number and do not show any agreement with either of the calculated variations. If a constant value of c_{dc} of 1.2 is assumed in the calculations of the theoretical characteristics, the agreement between the resulting theoretical variations and the experimental data is improved. (See fig. 7.) In fact, the differences between these theoretical results and the experimental results are about the same as those observed for the R-101 in figure 2 wherein the theoretical characteristics are appropriately based on a value of c_{dc} of 1.2. As with the tests of the Akron, the force tests of the RM-10 fuselage (fig. 8), which were conducted at several free-stream Mach numbers, do not show the expected erratic variation of the forces and moments and, in fact, the experimental data for this model are also in good agreement with the calculated values shown in figure 8 for which a constant value of c_{dc} of 1.2 was used.

The obvious inference that, contrary to reference 6, cross Reynolds number is not an important factor had to be viewed with some skepticism since the two bodies of revolution for which data were available were the type for which the radius varied continuously along the model length. As indicated by theory, the cross flow for such a body is more complex than that considered in the simple viscous theory since, as will be shown later, the large pressure recovery on the lee side of the body that is required by the theory for those sections

where the radius is decreasing with distance along the body influences the cross-flow characteristics to a large extent.

Because of this apparent anomaly, a special experiment was devised to further investigate the possible effects of cross Reynolds number on a body with a relatively long, constant-diameter section which might then be expected to exhibit the erratic variation of force and moment characteristics with angle of attack inferred from the circular-cylinder-section results. The body employed in these tests had an 11-inch length and was 1.5 inches in diameter. A short, nearly ogival nose was followed by a constant-diameter afterbody 7 inches long. Force and moment characteristics of this model were determined in the Ames 1- by 3-foot wind tunnels Nos. 1 and 2. The tests were run at two values of the free-stream Reynolds number. For the lower Reynolds number tests, the angle-of-attack range was such that the cross-flow Reynolds number based on maximum body diameter was always less than the critical value of approximately 2×10^5 . For the tests at the higher Reynolds number, the cross-flow Reynolds number exceeded the critical cross-flow Reynolds number at an angle of attack of approximately 5.5° . The results of the tests within the lower Reynolds number range, shown in figure 9(a), wherein the cross Reynolds numbers fall in the range for which the cross drag coefficient may be considered constant at a value of 1.2, show the expected smooth variation with angle of attack. The results for the higher Reynolds numbers, given in figure 9(b), show that an erratic variation with angle of attack of the lift, moment, and center-of-pressure position does occur although the actual values do not agree with the calculated characteristics. While these high Reynolds number tests do not indicate quantitative agreement with the calculated variation, they nevertheless serve to show that the cross Reynolds number can be important in determining the forces experienced.

Effect of Cross-Flow Mach Number

With the intent of comparing experimental and calculated characteristics on bodies for which the cross Mach number was large, the literature was again reviewed and it was found as before that little information was available. In the case of the 50-caliber shell of figure 10, the cross Mach number at the highest angle of attack was 0.7 which is well in excess of the critical Mach number. The curves representing viscous theory were calculated using, at each angle, the value of cross drag coefficient based on the actual cross Mach number. The experimental data on lift and drag increments are seen to agree closely with the calculated curve. It could be concluded that the allowance for high cross Mach number effects given by reference 6 was justified if it were not for the fact that the fineness ratio of the shell model was so low. For this model the agreement must be considered fortuitous.

In order to determine whether the suggested method is adequate for treating the slender body problem at high angles of attack where the cross Mach numbers are large, a series of models of various fineness ratios were tested to angles of attack such that the cross-flow Mach number exceeded unity. The models consisted of a 33-1/3 caliber, tangent ogival nose combined with various lengths of cylindrical afterbody so that the fineness ratios varied from 11.1 to 21.1. The theoretical curves used for comparison with the experimental data in figure 11 were calculated using equations (3) and the appropriate cross drag coefficient based on the actual cross-flow Mach number. The experimental lift- and drag-increment data show good agreement with the theoretical values. It is interesting to note that the lift-curve slope decreases at the extreme angles of attack in a manner similar to that which is indicated by the viscous theory if equations (2) rather than the simplified versions (equations (3)) are used. A curve showing the theoretical variation of lift coefficient based on equations (2) has been plotted in figure 11(a) for comparison. The variation of center-of-pressure position and of pitching moment with angle of attack shows that at the higher angles of attack the center of pressure is only slightly behind the position predicted by the viscous theory and that consequently the pitching moment, which in this case is about the nose of the model, is slightly more negative than predicted by the viscous theory. At the extreme angles of attack the experimental center-of-pressure positions are almost coincident with the centroid of plan-form area.

In review, the comparisons between theory and experiment in figures 2 to 11 have indicated that, in general, the lift and drag characteristics are fairly accurately predicted by the approximate viscous theory, but that designers must make some allowances for the fact that the actual center of pressure will be more rearward than the viscous theory would indicate. The variety of shapes of bodies used in these comparisons is sufficiently wide that the designer should be able to find one which is close to the design being considered and, accordingly, make a fair estimate of the discrepancies to be expected between the calculated and the actual centers of pressure for the particular case. An effect of cross Reynolds number in promoting erratic variations of forces in the critical cross Reynolds number range has been shown to exist on bodies with an appreciable length of constant diameter afterbody, but the actual variations depart considerably from the calculated characteristics. The information available on cross Mach number effects appears to support the suggested method from reference 6. Since the calculated and experimental force and moment characteristics differ, it is desirable to investigate the nature of the actual cross flow in some detail in order to determine wherein it differs from that assumed.

COMPARISON OF CALCULATED AND EXPERIMENTAL PRESSURE DISTRIBUTION
AND SOME OBSERVATIONS CONCERNING THE NATURE OF THE
INFLUENCE OF VISCOSITY

In order to show more clearly the manner in which the effects of viscosity influence the cross flow on inclined bodies of finite length, an experimental investigation of the pressure distributions for such bodies was made and the results compared with the theoretical distributions calculated on the assumption that the flow was inviscid. In reference 25, a method for calculating pressure distributions over slender inclined bodies of revolution in inviscid flow was given in which it was shown that the incremental pressure coefficient due to angle of attack for a slender body is given as (see fig. 15) ⁵

$$\Delta P = P - P_{\alpha=0} = 2 \tan \beta \cos \theta \sin 2\alpha + (1 - \sin^2 \theta) \sin^2 \alpha \quad (4)$$

The first term on the right-hand side of this equation is the contribution due to the change in cross-stream momentum resulting from the increase (or decrease) of radius with distance along the body, and the second term is the cross-flow contribution which would be obtained for a right circular cylinder in a stream moving at the cross stream velocity $V_0 \sin \alpha$. It can be seen from equation (4) that over the constant diameter portions of a body, for which $\tan \beta = 0$, the right-hand side of the equation reduces to the second term only and thus the theoretical incremental pressure distribution around this part of the body should be identical to that for a circular cylinder normal to a stream with the velocity $V_0 \sin \alpha$. It is well known that in this latter case, that is, steady-state two-dimensional flow around a circular cylinder, the large pressure recovery on the lee side of the cylinder that is required by theory cannot be realized. In a real viscous fluid, separation of the flow occurs and the actual pressure distribution exhibits far less pressure recovery than predicted by inviscid theory. In the calculation of forces by the method of reference 6, it is tacitly assumed that the actual circumferential pressure distributions deviate from the inviscid distributions in the same manner as for a circular cylinder. In figure 16(a) the experimental pressure distributions obtained at three stations on the inclined body shown in the figure are given. Also shown for comparison are the theoretical inviscid distribution and an experimental distribution on a circular cylinder section at the appropriate cross-flow Reynolds number (from reference 24). It is seen that the experimental distributions for the inclined body and the circular cylinder deviate from the inviscid distribution on the lee side in a

⁵The same formulas have been derived independently by Milton Van Dyke (see footnote 1, p. 3) and by Luidens and Simon in reference 26 using different methods of approach to the problem.

somewhat similar but not identical manner. A consideration of the development of the cross flow with distance along the body indicates the reasons for these observed differences.

Consider the development of the cross flow with respect to a coordinate system that is in a plane perpendicular to the axis of revolution of the inclined body. Let the plane move downstream with a velocity V_0 and let the coordinate system move within the plane such that the axis of revolution of the body is always coincident with the x axis of the coordinate system. The cross velocity is then $V_0 \sin \alpha$. At any instant during the travel of the plane from the nose to the base of the body, the trace of the body in the plane will be a circle and the cross-flow pattern within the plane may be compared with the flow pattern about a circular cylinder. Viewing the development of the cross flow in this plane for a body similar to that shown in figure 16, one would observe that as the plane moves from the nose toward the rear, the circular trace of the body on the plane would grow in size over the nose portion of the body and would be of constant diameter over the cylindrical afterbody. It might be anticipated that over the nearly constant diameter sections the development of the cross flow with distance along the body as seen in this moving plane would appear similar to that which would be observed for a circular cylinder impulsively set in motion from rest with a velocity $V_0 \sin \alpha$. Thus, the flow in the cross plane for the more forward sections should contain a pair of symmetrically disposed vortices on the lee side. Visual flow studies, which will be discussed later, showed that this cross-flow pattern did exist for the inclined body. The circumferential pressure distributions for these stations on the inclined body of revolution, therefore, should resemble those for a right circular cylinder which has been set in motion initially from rest and has moved only for a sufficient time to develop the symmetrical pair of vortices rather than the familiar Kármán vortex street which is eventually established. That this is the case is demonstrated by the comparison of pressure distributions in figure 16. In figure 16(a) are shown the experimental pressure distributions for a series of stations along the parallel section of the body of figure 11(c) at an angle of attack of 10.5° . These are compared with the pressure distributions in figure 16(b) obtained in a water channel by Schwabe (reference 27) on a right circular cylinder at several instants immediately after the cylinder had been impulsively set in motion from rest. The distance b from the "free stagnation point" (see fig. 16(b)), which moved downstream relative to the lee side of the cylinder, to the axis of revolution of the cylinder in terms of the body radius is shown for each of these pressure distributions. Downstream movement of this stagnation point is related with the downstream movement of the pair of vortices which is shown schematically in the sketch. A comparison of the series of pressure distributions for the inclined body of revolution with those for the right circular cylinder indicates general similarity.

In the more general case of a body for which the radius increases or decreases with distance along the body, the problem is further complicated. Theory indicates that the pressure to be recovered on those sections for which the radius increases with distance is less than would be required for the sections of constant diameter, while the converse is true for those sections where the radius is decreasing. Experimental pressure distributions for the body shown in figure 8 were obtained from reference 26 and are compared with the calculated distributions in figures 17, 18, and 19. At the station near the nose (fig. 17), not only is the theoretical pressure recovery small but the cross-flow boundary layer has had little distance in which to develop. Thus it is not surprising that the experimental pressure distributions are in good agreement with those calculated using the inviscid theory. In figure 18 is shown a similar comparison for the station of maximum diameter. Here the theoretical pressure recovery is increased and the cross-flow boundary layer has had time to develop. In consequence, separation of the cross-flow boundary layer has started on the lee side of the body. In figure 19 is shown the comparison at a station near the base. Here the separation has progressed to nearly the 90° point. Experimental measurements of the flow field near the base of this body (reference 26) as well as visual-flow studies have demonstrated that for this body at angles of attack less than approximately 15° there is a pair of symmetrically disposed vortices formed on the lee side similar to that formed for the body of figure 16(a).

Visual Flow Studies

To further investigate the formative stages of such cross flows, the body of figure 11(c) was studied in both a free-surface water tank and the 1- by 3-foot supersonic wind tunnel. In the water tank shown in figure 20, the model is mounted on a motor-driven carriage shown in the figure. The model may be moved in or out of the water in a direction normal to the free surface of the water and can be set at any arbitrary angle of attack. The motion of the free surface of the water, which indicates the nature of the cross flow, can then be studied as the model is driven below the surface. In the wind tunnel use was made of a technique which has been termed the "vapor screen method." With this technique the cross flow is made visible in the following manner (see fig. 21): A small amount of water, which condenses in the wind-tunnel test section to produce a fine fog, is introduced into the tunnel air stream. A narrow plane of bright light, produced by a high-pressure mercury-vapor lamp, is made to shine through the glass window in a plane essentially perpendicular to the axis of the tunnel. In the absence of the model this plane appears as a uniformly lighted screen of fog particles. When the model is put in place at any arbitrary angle of attack the result of any disturbances in the flow produced by the model which affects the amount of light scattered by the water particles in this lighted plane can be seen and photographed.

By the use of the free-surface method of studying cross flow in the water tank and the vapor screen method for studying the cross flow on the same model in the wind tunnel, some interesting facts concerning the nature of the cross flow have been found. The two techniques showed similar results. At angles of attack up to nearly 20° the wind tunnel and the water tank showed that over the length of this body, progressing downstream from the bow, a pair of symmetrically disposed vortices was formed on the lee side similar to that shown in reference 27 for the cylinder a short time after having been set impulsively in motion from rest. The vortices were of greater strength and separated farther from the body at the stations near the base. A typical set of pictures illustrating these vortices in the water tank and in the wind tunnel are shown in figure 22 for an angle of attack of 15° . In the water tank tests these vortices were made evident in the photograph by aluminum powder carried into the fluid from the body surface. In the wind tunnel the vortices made themselves evident as black dots on the vapor screen due to the absence of scattered light which is believed to result from the action of the vortices in spinning the fine droplets of fog out of the fast-turning vortex cores. It is of interest to note in the wind-tunnel picture (this is more clearly seen than photographed) that the section through the Mach cone from the bow is also evident as a circular zone of slightly stronger light intensity.

A similar comparison of the results from the water tank and the wind tunnel was again made for 35° angle of attack. At such a large angle the following characteristic cross flow was obtained: The symmetrically disposed vortices were formed at first in the section on and immediately following the ogival nose. A short distance downstream this unstable configuration of vortices promoted the familiar street of alternate vortices characteristic of the steady-state flow known to exist behind a circular cylinder section. (See, for instance, reference 27.) The vortices discharged from the inclined body of revolution had their cores alined in nearly the free-stream direction. In figure 23 are shown photographs of the cross flow on this same body at 35° angle of attack at a station near the base. Again the water tank free surface indicated a discharged vortex street similar to that observed in the wind tunnel. It is of interest to point out that in these wind-tunnel tests the distribution of the discharged vortices was aperiodically reversed. That is to say, the discharged vortex closest to the body would at one instant be on one side of the body and at the next instant, perhaps several seconds later, on the other. No regularity in this change in the distribution of the vortex street has as yet been found.

The pressure distributions of figure 16 and the experiments with flow visualization constitute the most convincing demonstration that the development of the cross flow with distance along the body on a long inclined body of constant diameter behaves much the same as the

development with time of the flow on a circular cylinder impulsively set in motion from rest. It is known (see references 24 and 27) that the drag of a circular cylinder impulsively set in motion from rest at first rises rapidly to a drag coefficient greater than 2.0 and with continued motion subsides to the steady-state value of 1.2. Thus, it appears that the cross-flow drag coefficient for the inclined body should start at zero at the nose, increase with distance along the body to a value in excess of the steady-state value for a circular cylinder, and for long bodies at high angles of attack, fall to or near the average steady state value over the afterportion of the body. Since this variation of cross-flow drag coefficient would yield a total cross force approximating that which would be predicted on the assumption that the cross-flow drag coefficient is constant along the body, it is not surprising that the integrated lift and drag increment due to inclination of the body are in good agreement with the calculated values based on this latter assumption and that the calculated center of pressure is closer to the nose than is the actual center of pressure.

Since the cross flow over the elements of the body near the bow corresponds to the nonsteady-state-flow condition that exists on a circular cylinder, the critical cross Reynolds number, if such exists for these elements, would not necessarily be expected to be the same as that for the steady-state flow over such a cylinder. Thus from this cause alone it is not surprising that the calculated force and moment characteristics for bodies in which the cross-flow Reynolds number is in the critical Reynolds number range for a two-dimensional circular cylinder are not in good agreement with the observed characteristics. The contention of reference 6 that some erratic force and moment behavior may be expected in this range of cross-flow Reynolds numbers for long bodies is nevertheless supported.

Another point which may be of considerable importance to missile designers is that on very long missiles designed to operate to large angles of attack the discharge of a vortex street should promote asymmetry of forces on the tail surfaces and manifest itself as a tendency to unexpected and erratic rolling on a configuration for which the flow might ordinarily be expected to be perfectly symmetrical. Moreover, the aperiodic changes in the discharged street of vortices might induce for a pitched body undesirable forces and moments in yaw.⁶

Throughout this paper only bodies of revolution have been considered. Designers, for certain applications, might employ bodies of other than circular section to advantage. For example, for winged configurations which must operate at large angles of attack and for which

⁶Some recent investigations in the Ames 6- by 6-foot supersonic wind tunnel on a body-tail combination have shown that such fluctuating forces and moments do occur.

inclined flight occurs essentially in only one plane, the use of a streamlined body cross section in order to avoid the formation of lee-side vortices and possible adverse effects when shed as a street might be desirable. Another example is the use of a body with a flat surface on the windward side which might prove valuable in increasing the cross-flow drag coefficient and thus the body contribution to the lift-curve slope. However, flight with this type of body would have to be confined to small angles of attack to avoid adverse effects attendant to the shedding of the vortices from the body.

Ames Aeronautical Laboratory,
National Advisory Committee for Aeronautics,
Moffett Field, Calif.

APPENDIX A

SYMBOLS

A	reference area for coefficient evaluation
A_p	plan-form area
c_{dc}	drag coefficient which would be experienced by a circular cylinder section of radius r at Reynolds number and Mach number based upon the diameter and the cross component of velocity ($V_0 \sin \alpha$)
C_D	total-drag coefficient
C_{DB}	base-drag coefficient
C_{DF}	fore-drag coefficient $(C_D - C_{DB})$
ΔC_D	incremental drag coefficient $[C_D - (C_D)_{\alpha=0}]$
ΔC_{DF}	incremental fore-drag coefficient $[C_{DF} - (C_{DF})_{\alpha=0}]$
C_L	lift coefficient
C_M	pitching-moment coefficient, in terms of reference area A and reference length l
d	maximum body diameter
f	local cross force per unit length
k_1	longitudinal apparent mass coefficient
k_2	transverse apparent mass coefficient
l	body length
M	Mach number
M_c	cross Mach number $(M \sin \alpha)$
P	pressure coefficient at angle of attack
$P_{\alpha=0}$	pressure coefficient at zero angle of attack

ΔP	incremental pressure coefficient due to angle of attack ($P - P_{\alpha=0}$)
q	free-stream dynamic pressure
r	local body radius
Re	free-stream Reynolds number (based on diameter)
Re_c	cross-flow Reynolds number ($Re \sin \alpha$)
s	local cross-sectional area
S_b	area of the base
V_0	free-stream velocity
vol	volume of the body
x	distance along the body
x_m	distance to the ^{chosen} moment center from the nose
x_p	distance to the centroid of plan-form area from the nose
X	reference length for coefficient evaluation
α	angle of inclination
β	$\tan^{-1} (dr/dx)$
η	ratio of the drag coefficient of a circular cylinder of finite length to that of a circular cylinder of infinite length
θ	polar angle about axis of revolution measured from the approach direction of the cross-stream velocity

APPENDIX B


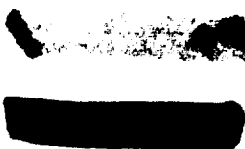
EFFECTS OF MACH NUMBER AND REYNOLDS NUMBER ON THE VALUE OF η

The only experimental data available (reference 24) for the evaluation of η , the ratio of the drag coefficient of a circular cylinder of finite length to that of a circular cylinder of infinite length, have been reproduced in figure 14. These data are for a negligibly low Mach number and for a single Reynolds number (88,000) which corresponds to the Reynolds number range for which 1.2 is the drag coefficient of a cylinder of infinite length. To obtain a rough estimate of the value of η at other Reynolds and Mach numbers the following conjecture is given: The primary end-relieving effect for a cylinder of finite length must be conveyed to other sections through the low-velocity regions of the wake since it is this low-energy flow behind the cylinder which is most susceptible to alteration due to pressure differences in the vicinity of the ends of the cylinder. Evidently the ratio of the spanwise length of the wake to the wake thickness would be the ratio that should determine η . The spanwise length of the wake will be approximately the length of the cylinder, while the wake thickness will be nearly proportional to the product of the cylinder diameter and the drag coefficient. It appears, then, that the value of η at Reynolds and Mach numbers for which c_{dc} is not 1.2 might be taken as the value of η (from fig. 14) for an effective cylinder length-to-diameter ratio equal to the product of the actual length-to-diameter ratio and the ratio of the drag coefficient 1.2 to the section drag coefficient at the Reynolds and Mach number of the case considered.

REFERENCES

1. Munk, Max.: The Aerodynamic Forces on Airship Hulls. NACA Rep. 184, 1924.
2. Ward, G. N.: Supersonic Flow Past Slender Pointed Bodies. Quarterly Jour. of Mechanics and Applied Mathematics, vol. 2, part I, Mar. 1949, pp. 75-97.
3. Harrington, R. P.: An Attack on the Origin of Lift of an Elongated Body. Daniel Guggenheim Airship Institute, Publication 2, 1935.
4. Tsien, Hsue-Shen: Supersonic Flow Over an Inclined Body of Revolution. Jour. Aero. Sci., vol. 5, no. 12, Oct. 1938, pp. 480-483.
5. Jones, R. T.: Effects of Sweepback on Boundary Layer and Separation. NACA Rep. 884, 1947.
6. Allen, H. Julian: Estimation of the Forces and Moments Acting on Inclined Bodies of Revolution. NACA RM A9126, 1949.
7. Jones, R., and Bell, A. H.: Experiments on a Model of the Airship R. 101. R. & M. No. 1168, British A.R.C., Sept. 1929.
8. Jones, J. Lloyd, and Demele, Fred A.: Aerodynamic Study of a Wing-Fuselage Combination Employing a Wing Swept Back 63° . Characteristics Throughout the Subsonic Speed Range With the Wing Cambered and Twisted for a Uniform Load at a Lift Coefficient of 0.25. NACA RM A9D25, 1949.
9. Turner, Robert L., Jr.: Stability and Control Tests of a 0.135-Scale XAAM-N-2 Model in the 19- x 27.5-Inch Mach 1.50 Nozzle. OAL Rep. 112-4, Aug. 1949.
10. Gardenier, H. E.: Stability and Control Tests of a 0.135-Scale XAAM-2 Model in the 19- x 27.5-Inch, M 1.73 Nozzle. OAL Rep. 112, Sept. 1948.
11. Turner, Robert L., Jr.: Stability and Control Tests of a 0.135-Scale XAAM-N-2 Model in the 19- x 27.5-Inch Mach 2.50 Nozzle. OAL Rep. 112-5, Aug. 1949.
12. Turner, Robert L., Jr.: The Effect of Surface Roughness of Various Model Components on Stability and Control Characteristics of the 0.135-Scale Sperry XAAM-N-2 Model at M - 2.24. OAL Rep. 112-7, Sept. 1949.

13. Peters, R. G.: Data Report for Supersonic Wind Tunnel Tests on GAPA Model FR-87 Fifth Aberdeen Test Period, $M = 1.72$. Boeing Document D-8397 (Tech. Rep. No. 111-7). Aug. 1947.
14. Peters, R. G.: Data Report for Supersonic Wind Tunnel Tests on GAPA Model FR-87 Sixth and Seventh Aberdeen Test Periods, $M = 1.72$ and $M = 1.28$. Boeing Document D-8788 (Tech. Rep. No. 111-9). Feb. 1948.
15. Freeman, Hugh B.: Force Measurements on a $1/40$ -Scale Model of the U. S. Airship "Akron". NACA TR 432, 1932.
16. Esenwein, Fred T., Obery, Leonard J., and Schueller, C. F.: Aerodynamic Characteristics of NACA RM-10 Missile in 8- by 6-foot Supersonic Wind Tunnel at Mach Numbers from 1.49 to 1.98. - II Presentation and Analysis of Force Measurements. NACA RM E50D28, 1950.
17. Anon.: Supersonic Wind Tunnel Tests of Small Caliber Projectiles: Cal. .50 API M23; Cal. .60 API T39; and 20mm HEI M97. Aberdeen BRL Tech. Note No. 11, June 30, 1949.
18. von Kármán, Th.: The Problem of Resistance in Compressible Fluids. Roma, Real Accademia D'Italia, 1935-XIV.
19. Lindsey, W. F.: Drag of Cylinders of Simple Shapes. NACA Rep. 619, 1938.
20. Stack, John: Compressibility Effects in Aeronautical Engineering. NACA ACR, 1941.
21. Relf, E. F.: Discussion of the Results of Measurements of the Resistance of Wires, With Some Additional Tests on the Resistance of Wires of Small Diameter. R. & M. No. 102, British A.C.A., 1914.
22. Wieselsberger, C.: New Data on the Laws of Fluid Resistance, NACA TN 84, 1922.
23. Stanton, T. E.: On the Effect of Air Compression on Drag and Pressure Distribution in Cylinders of Infinite Aspect Ratio, R. & M., No. 1210, British A.R.C., Nov. 1928.
24. Goldstein, S.: Modern Developments in Fluid Dynamics. Oxford, The Clarendon Press, vol. II, 1938, pp. 419-421.

- 
25. Allen, H. Julian: Pressure Distribution and Some Effects of Viscosity on Slender Inclined Bodies of Revolution. NACA TN 2044, 1950.
26. Luidens, Roger W., and Simon, Paul C.: Aerodynamic Characteristics of NACA RM-10 Missile in 8- by 6-foot Supersonic Wind Tunnel at Mach Numbers From 1.49 to 1.98. I - Presentation and Analysis of Pressure Measurements (Stabilizing Fins Removed). NACA RM E50D10, 1950.
27. Schwabe, M.: Pressure Distribution in Nonuniform Two-Dimensional Flow. NACA TM 1039, 1943.
- 

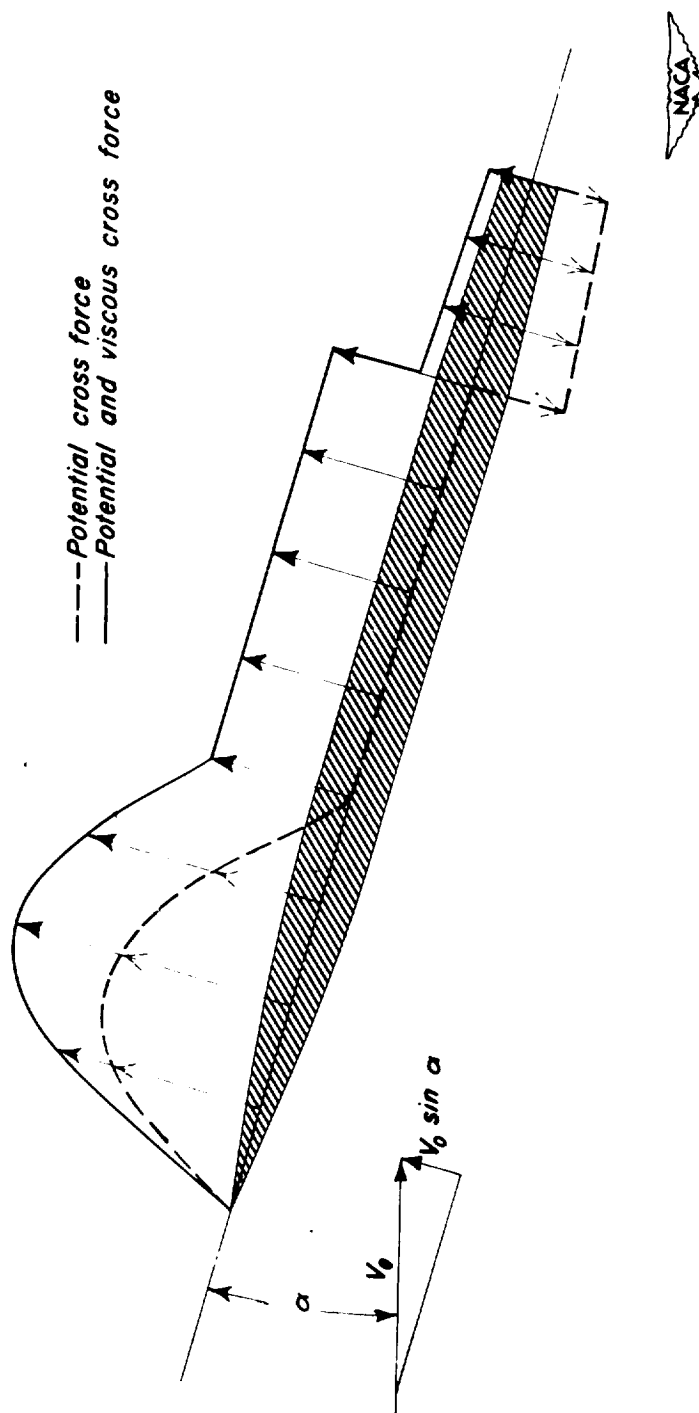


Figure 1.— Schematic diagram of the theoretical cross-force distribution on a body of revolution.

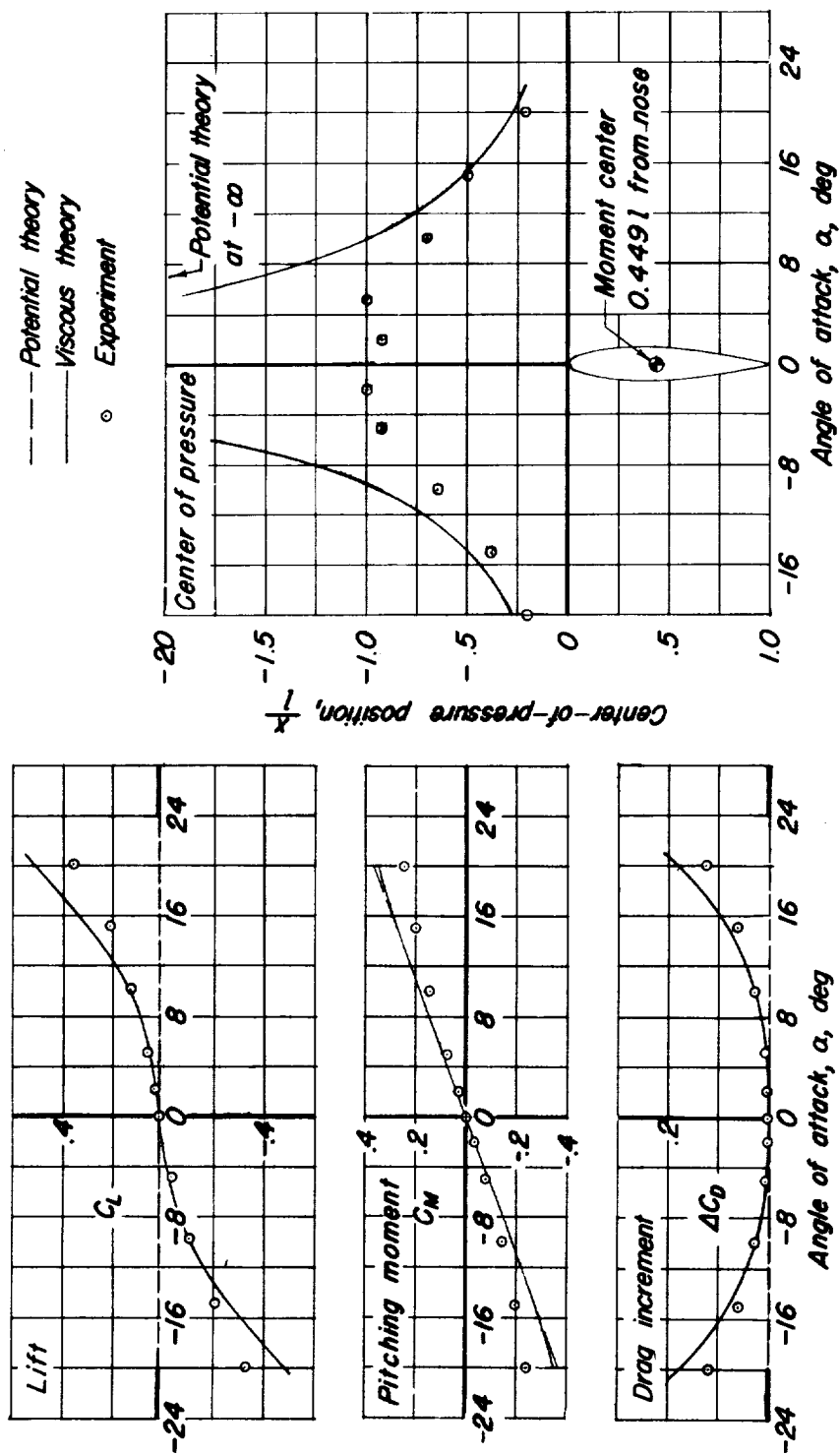


Figure 2.-Lift, pitching-moment, drag, and center-of-pressure variations for R-101 (reference 7).

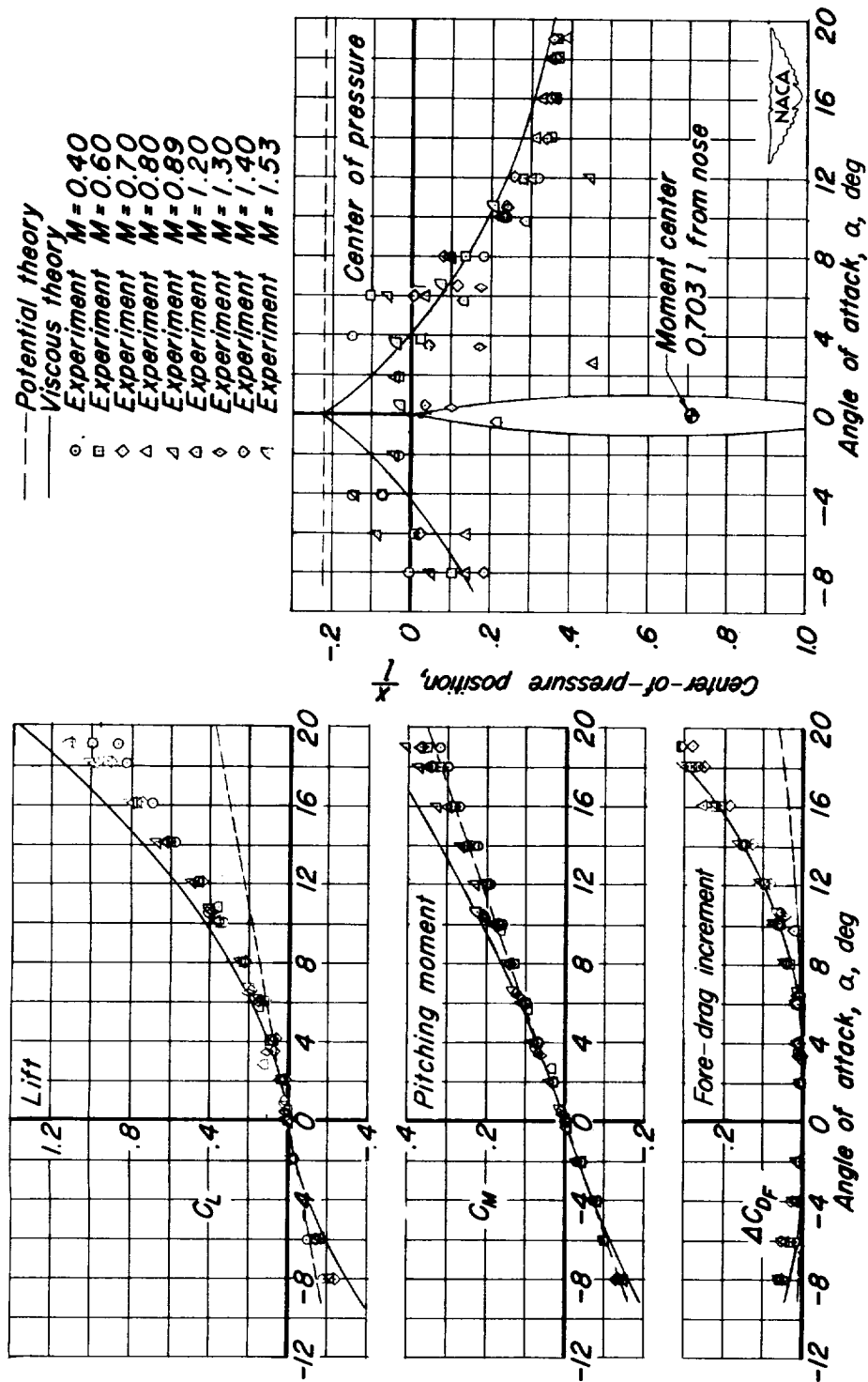


Figure 3.- Lift, pitching-moment, drag, and center-of-pressure variations on body of revolution (reference 8).

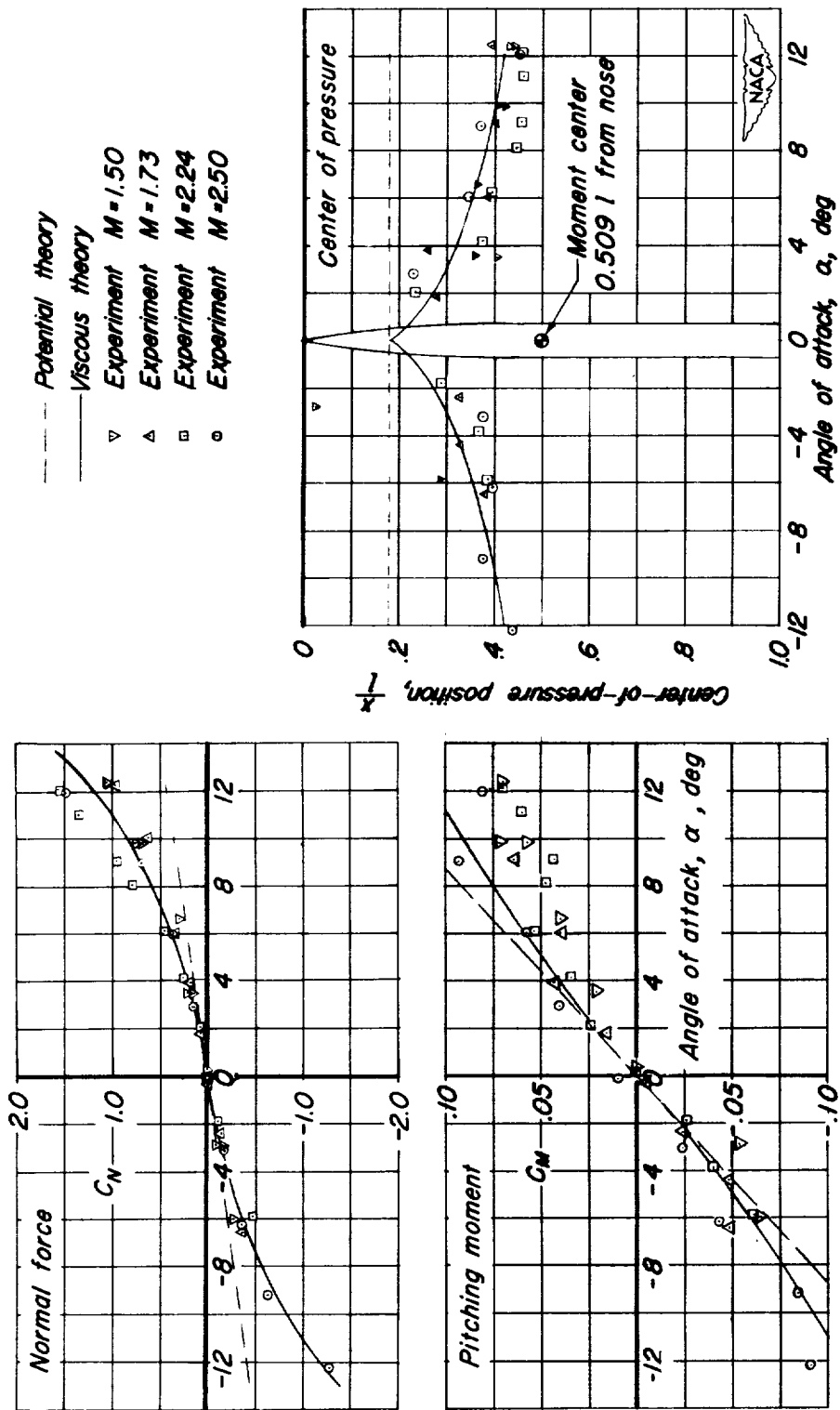


Figure 4. - Normal-force, pitching-moment, and center-of-pressure variations for Sparrow (references 9, 10, 11, 12).

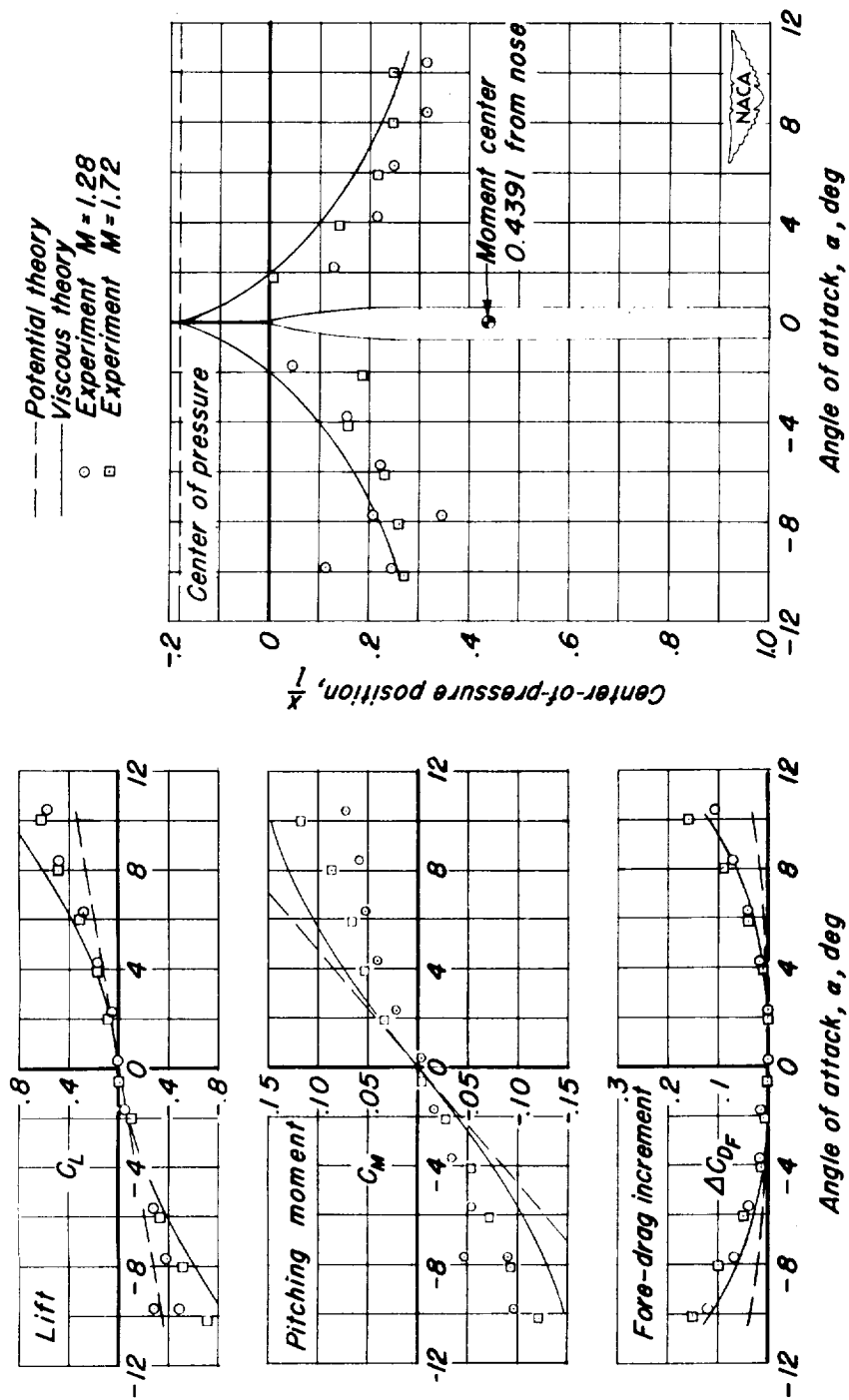


Figure 5. - Lift, pitching-moment, drag, and center-of-pressure variations for Gapa FR-87 (references 13 and 14)

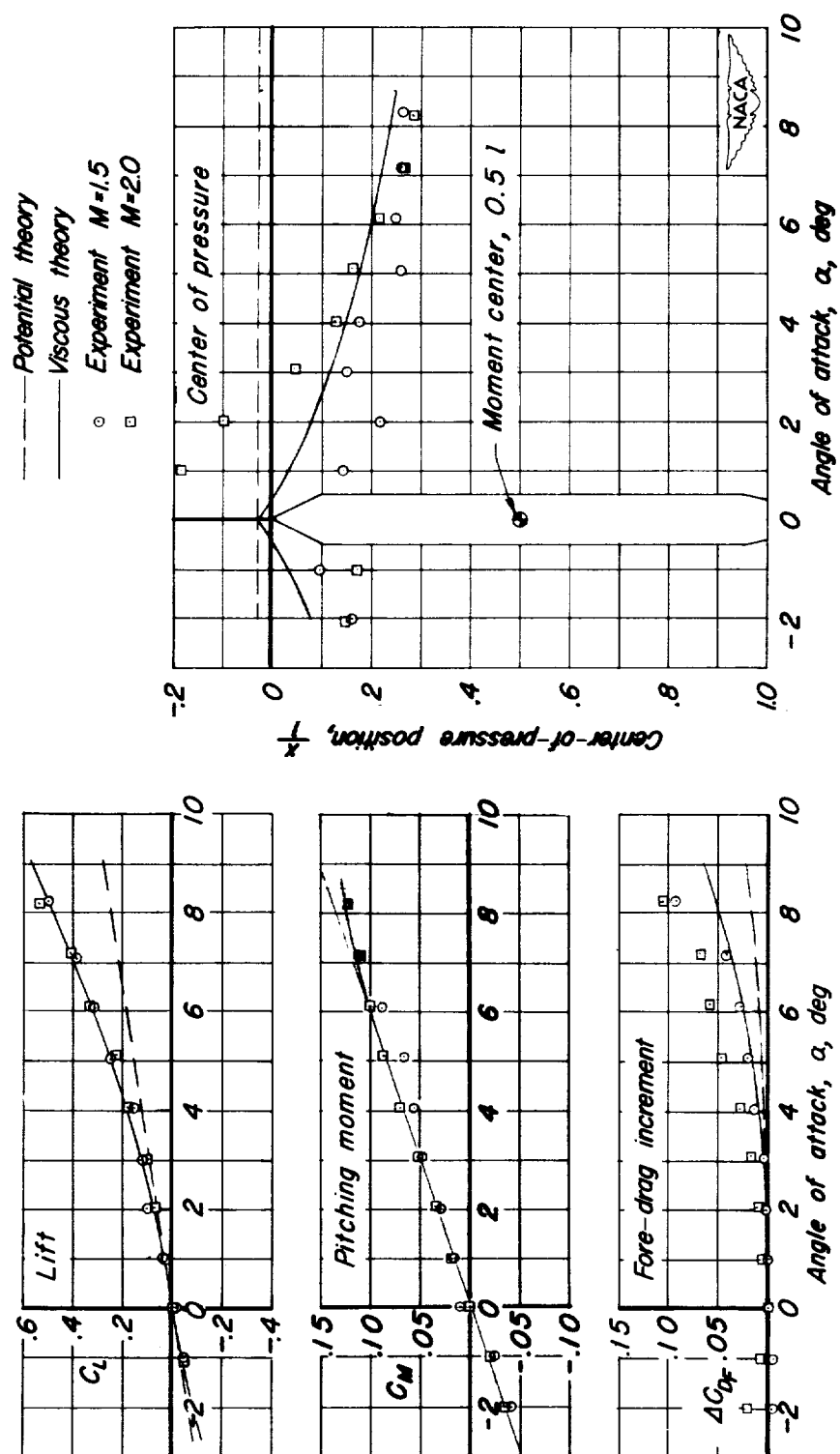


Figure 6. - Lift, pitching-moment, drag, and center-of-pressure variations for Rigel (AAL 1-by3-foot W.T.).

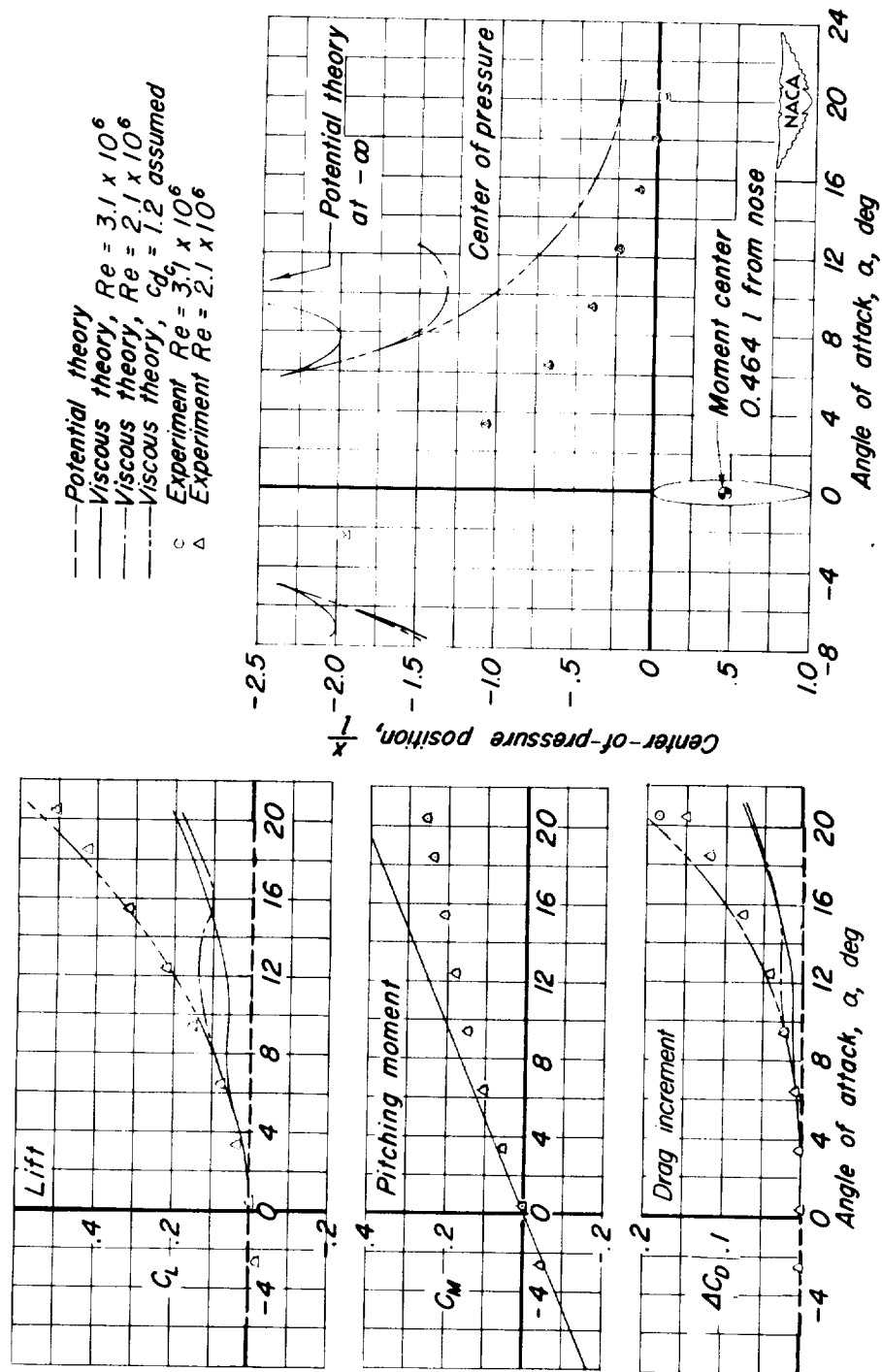


Figure 7. - Lift, pitching-moment, drag, and center-of-pressure variations for airship U.S.S. Akron (reference 15).

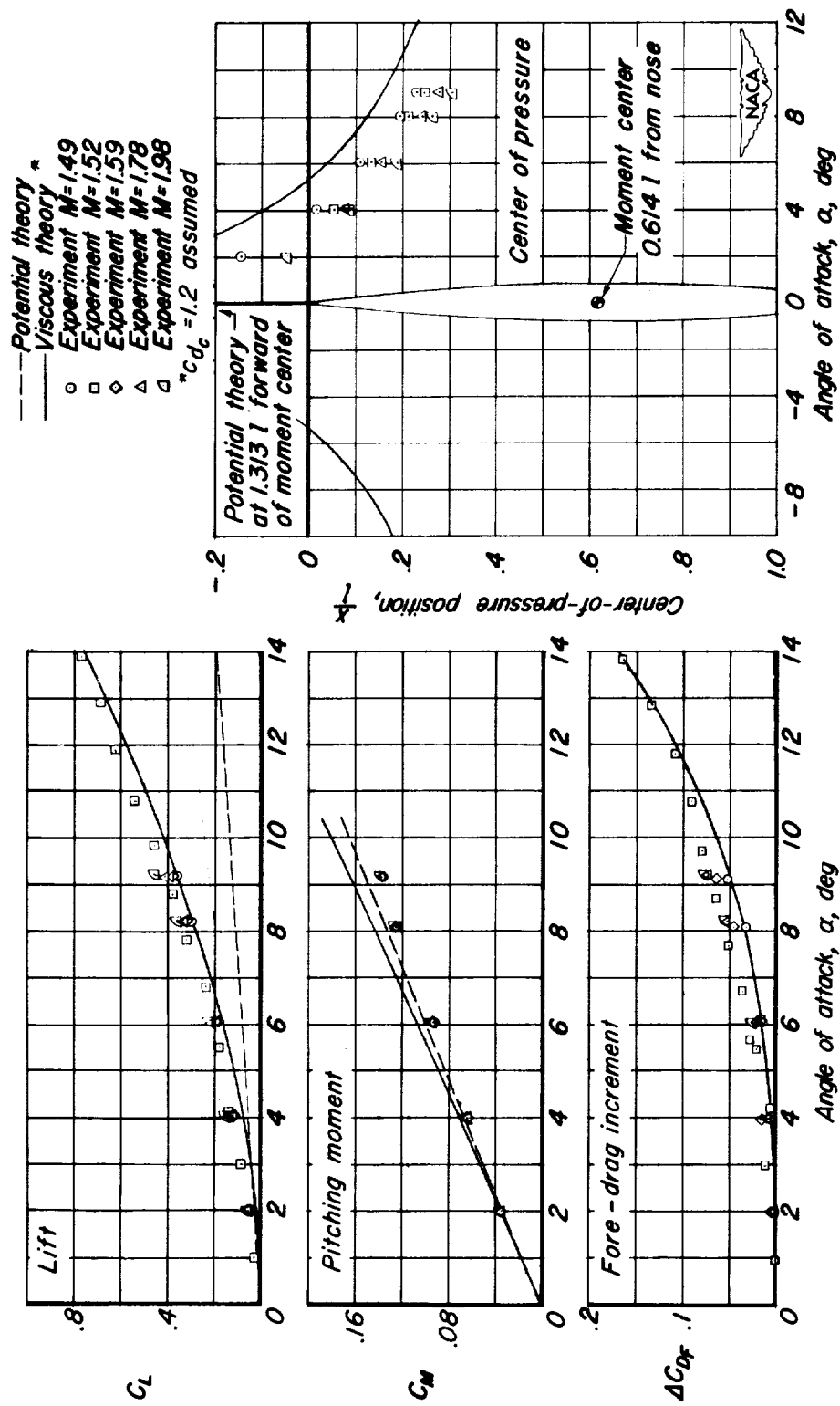


Figure 8.—Lift, pitching-moment, drag, and center-of-pressure variations for RM-10 (reference 16).

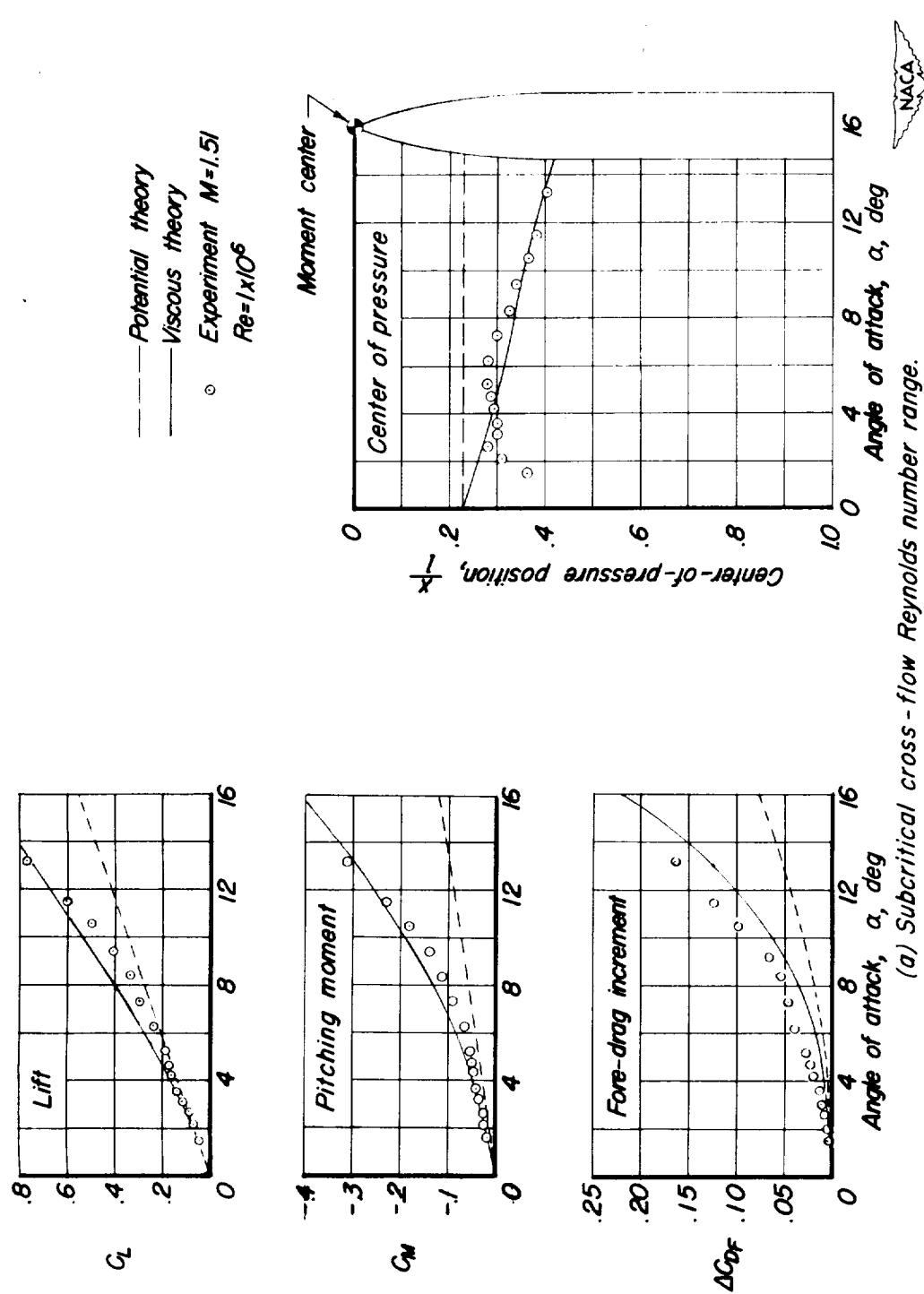


Figure 9. - Experimental and theoretical characteristics of a body of revolution in the subcritical and critical cross-flow Reynolds number range (AAL 1-by3-foot W.T.).

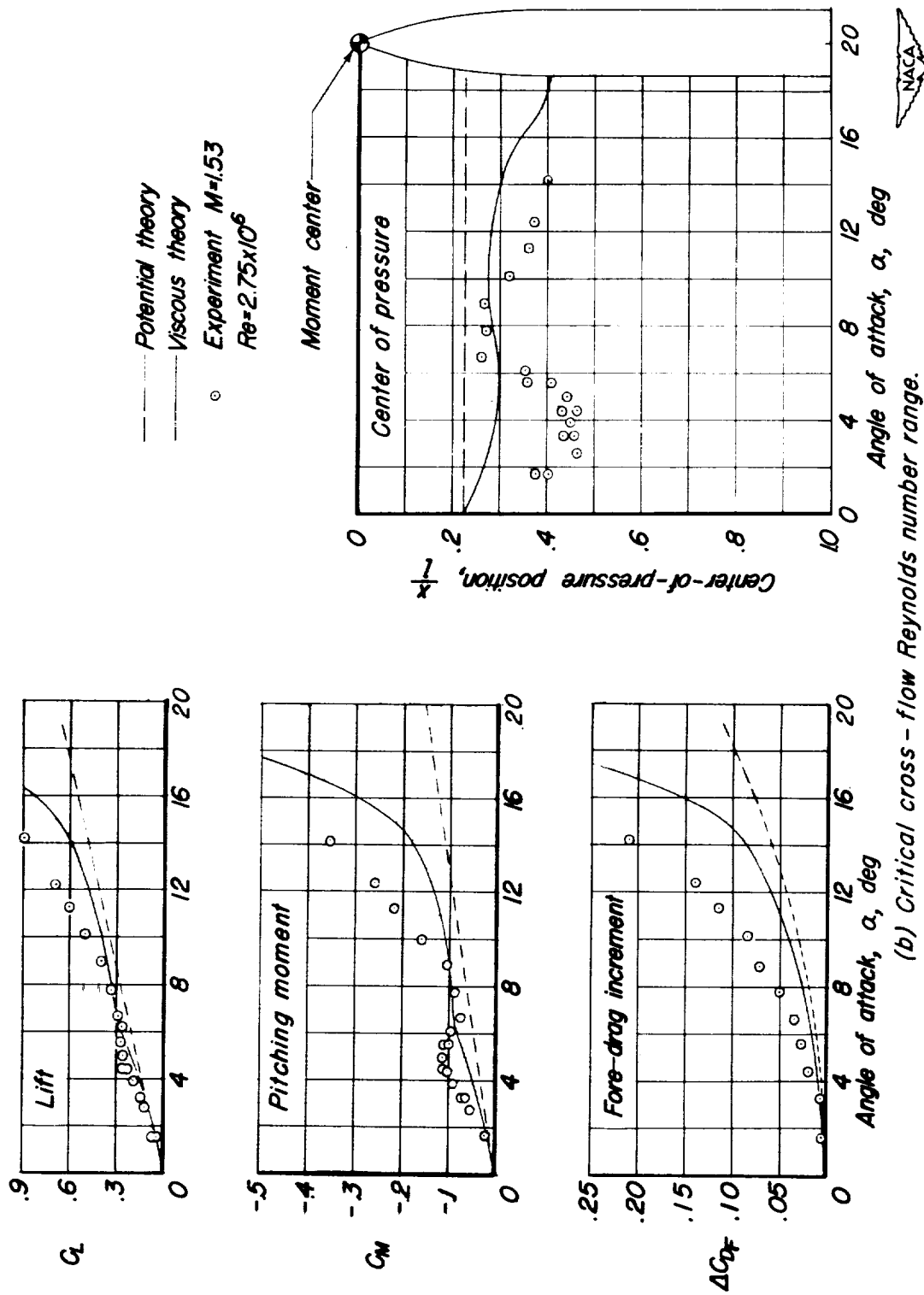


Figure 9. - Concluded.

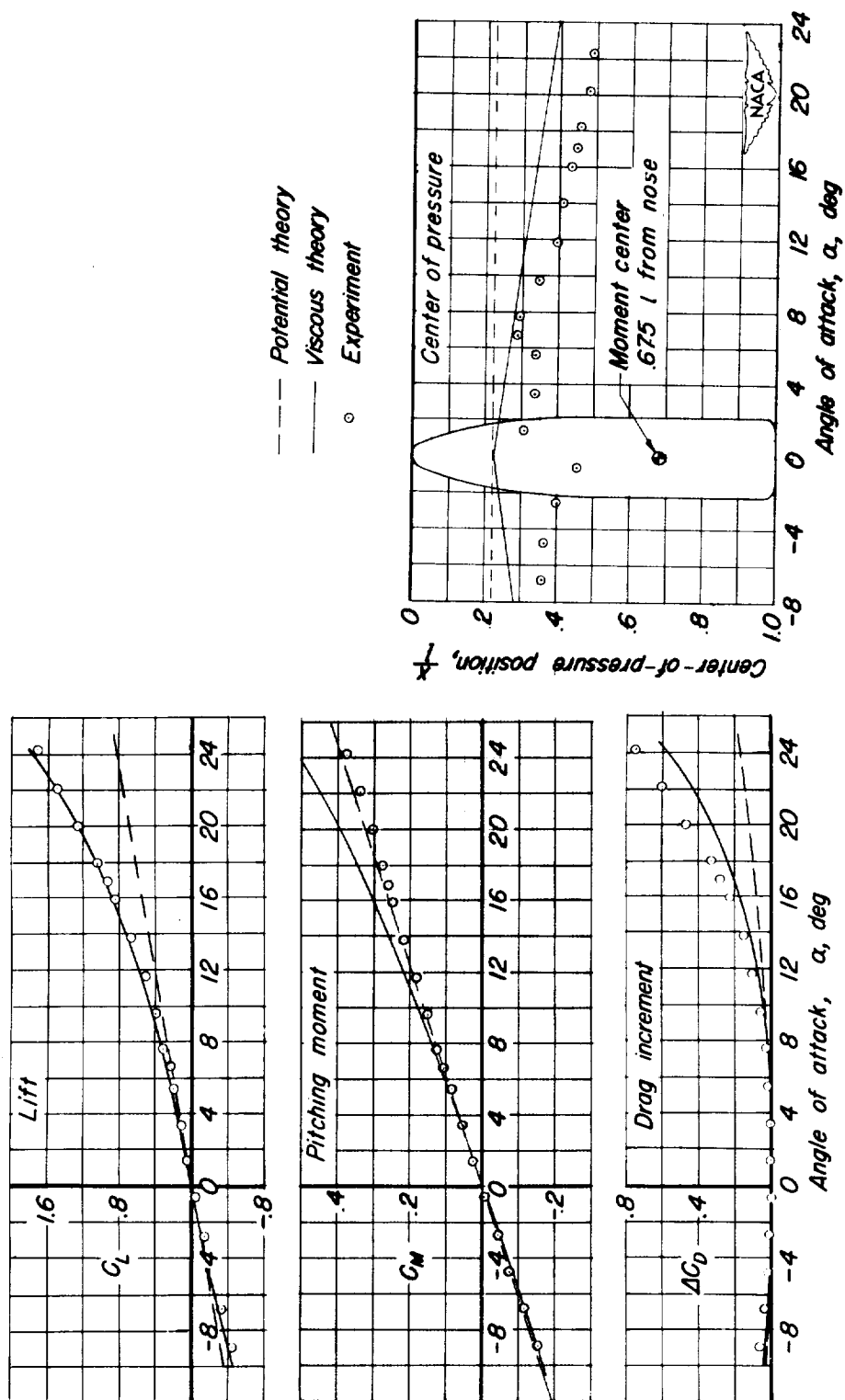


Figure 10.- Lift, pitching-moment, drag, and center-of-pressure variations for 50 caliber shell (reference 17).

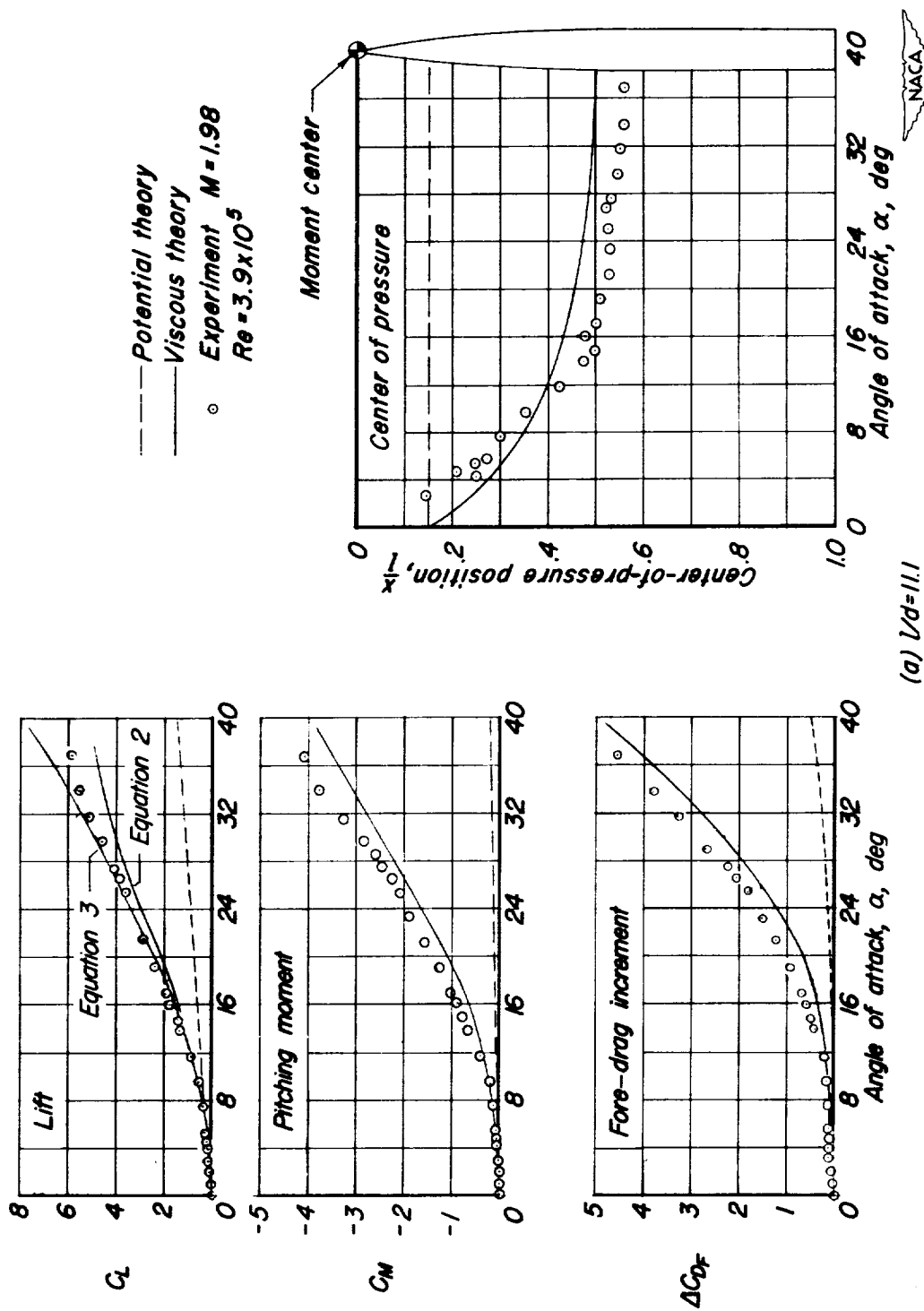
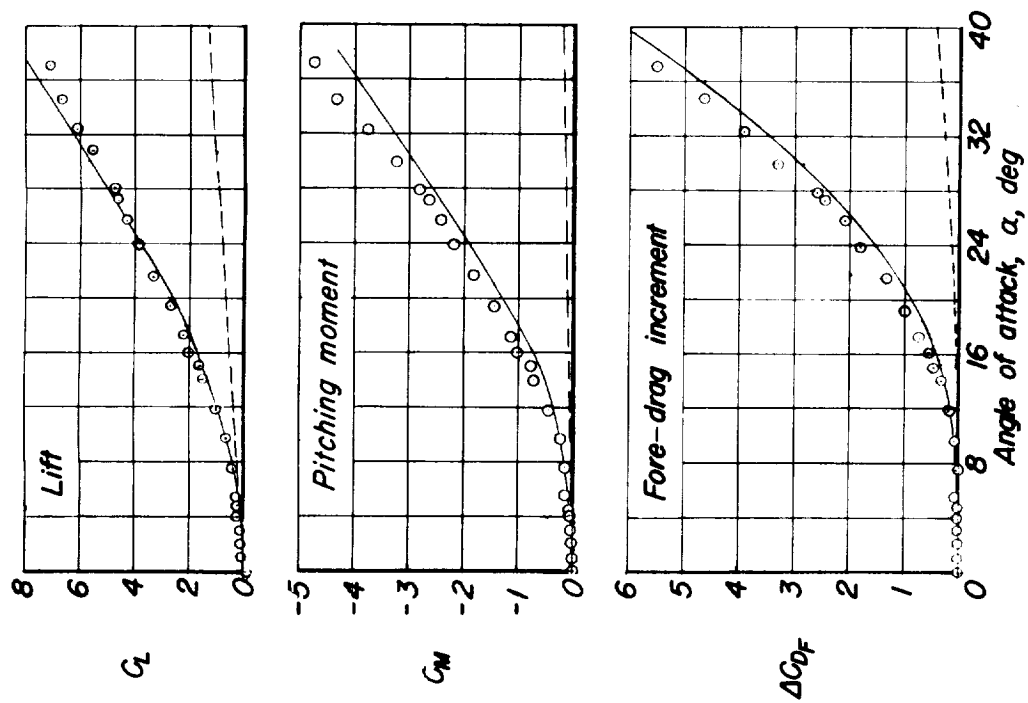
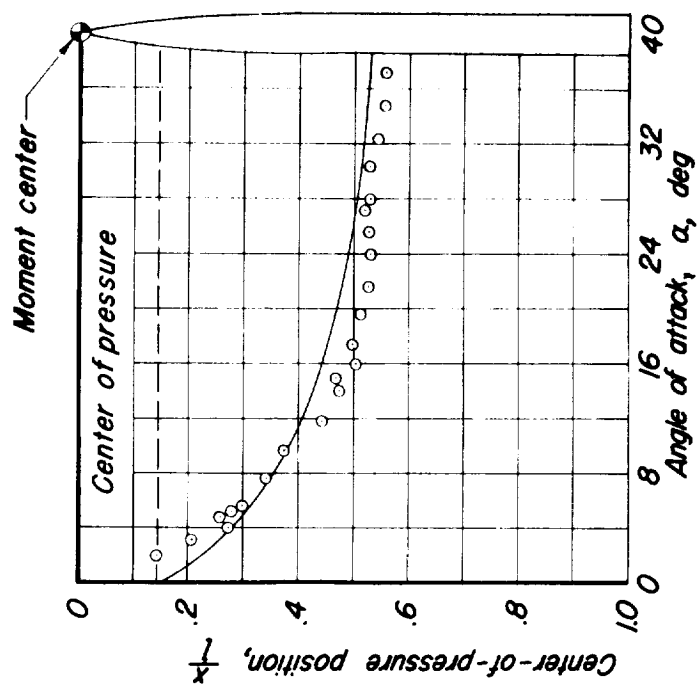


Figure 11.—Lift, pitching-moment, fore-drag increment, and center-of-pressure variations for a family of bodies of revolution (AAL 1-by3-foot W.T.).



--- Potential theory
 --- Viscous theory
 ○ Experiment $M=1.98$
 $Re=3.9 \times 10^5$



(b) $l/d=13.1$

Figure 11. —Continued.

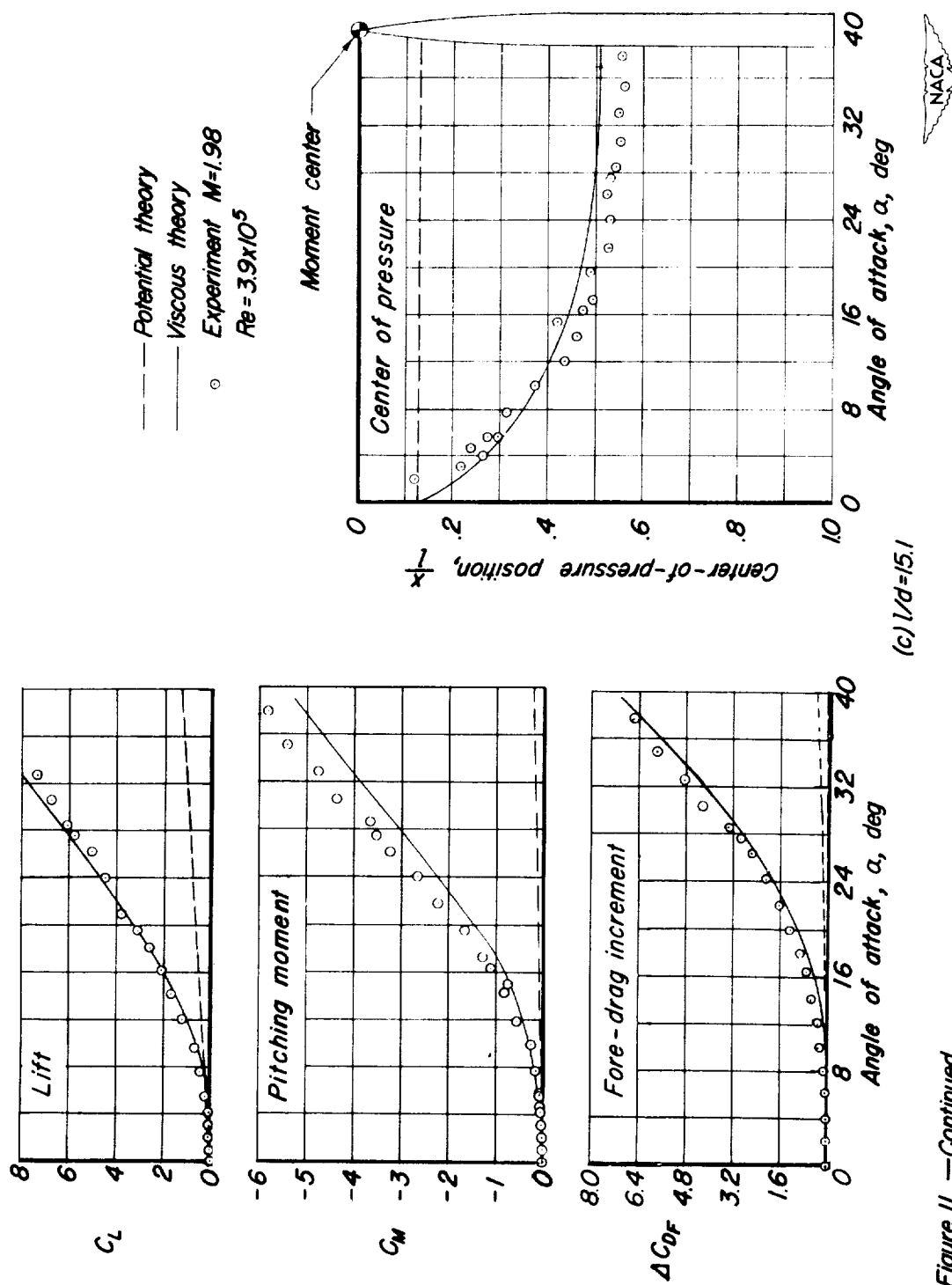


Figure 11. —Continued.

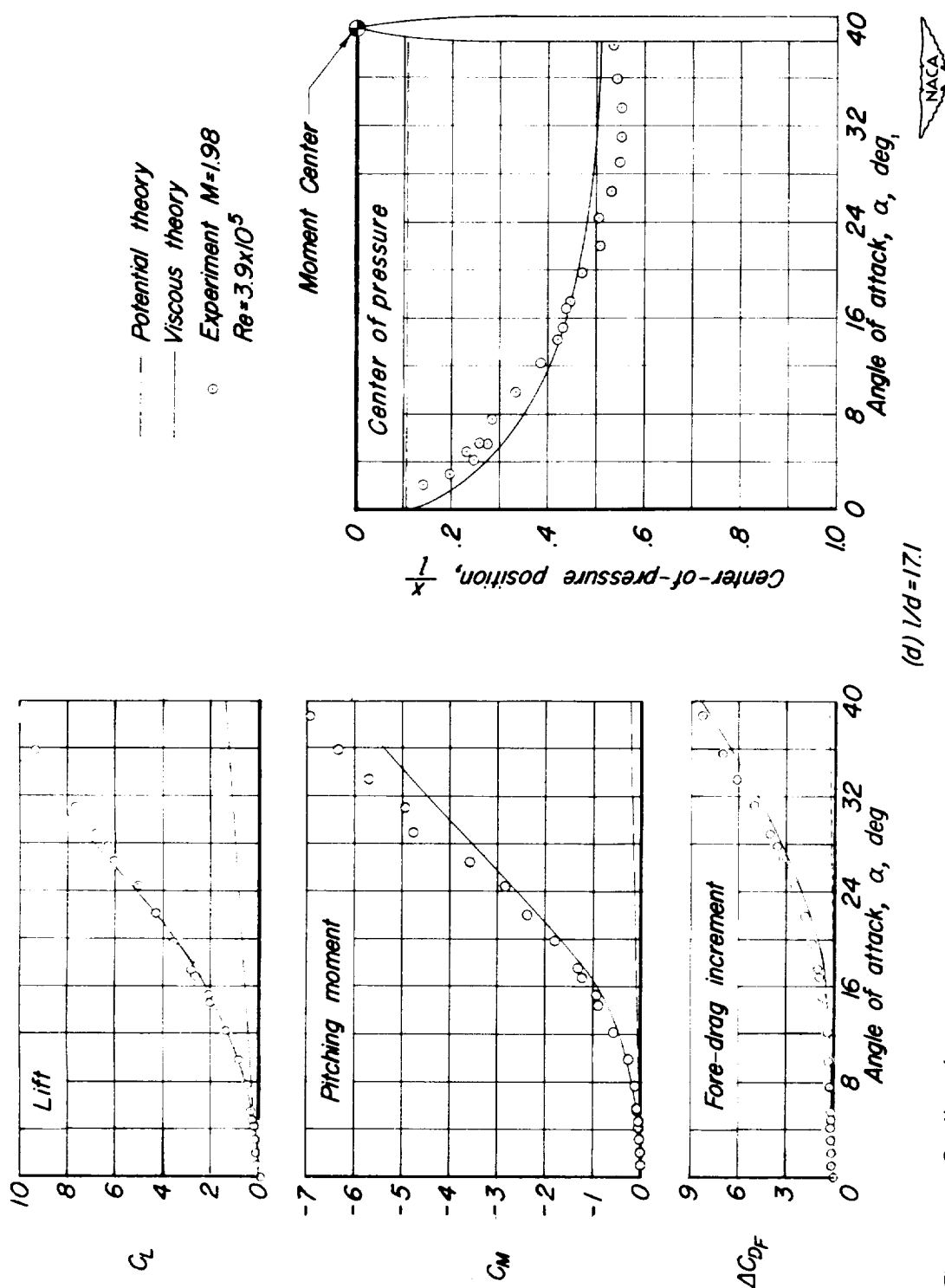


Figure 11. — Continued.

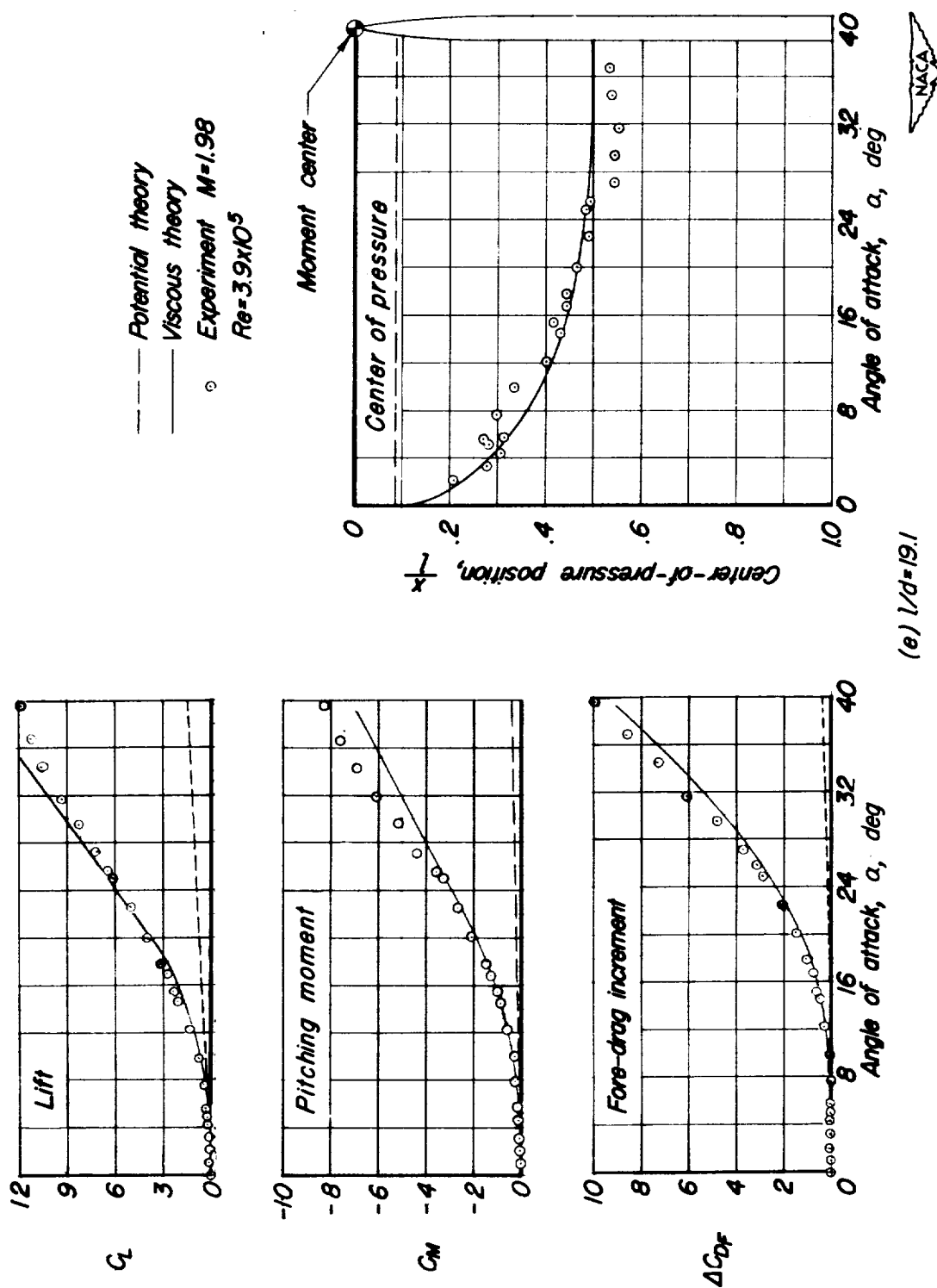


Figure 11. —Continued.

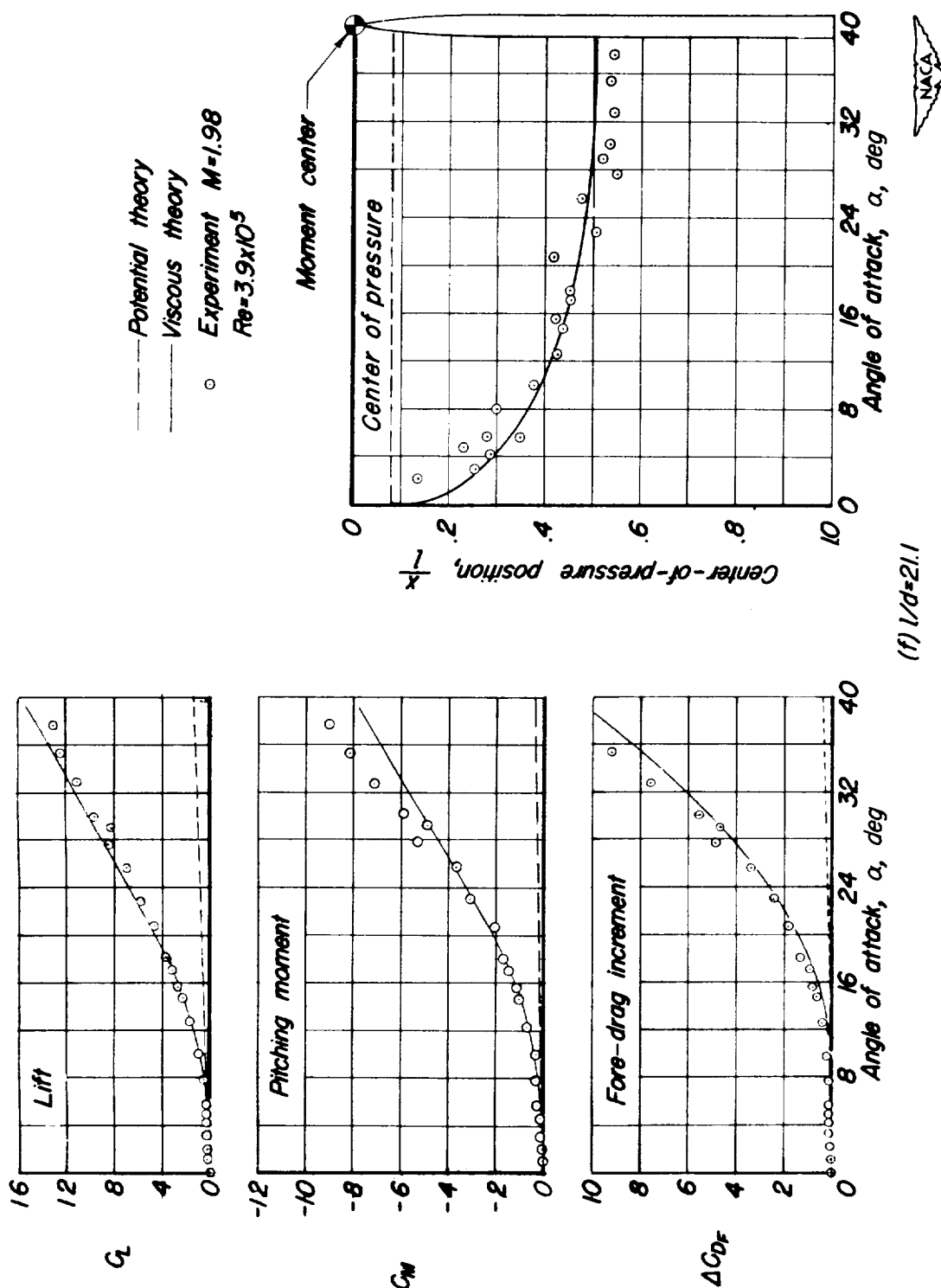


Figure 11. — Concluded.

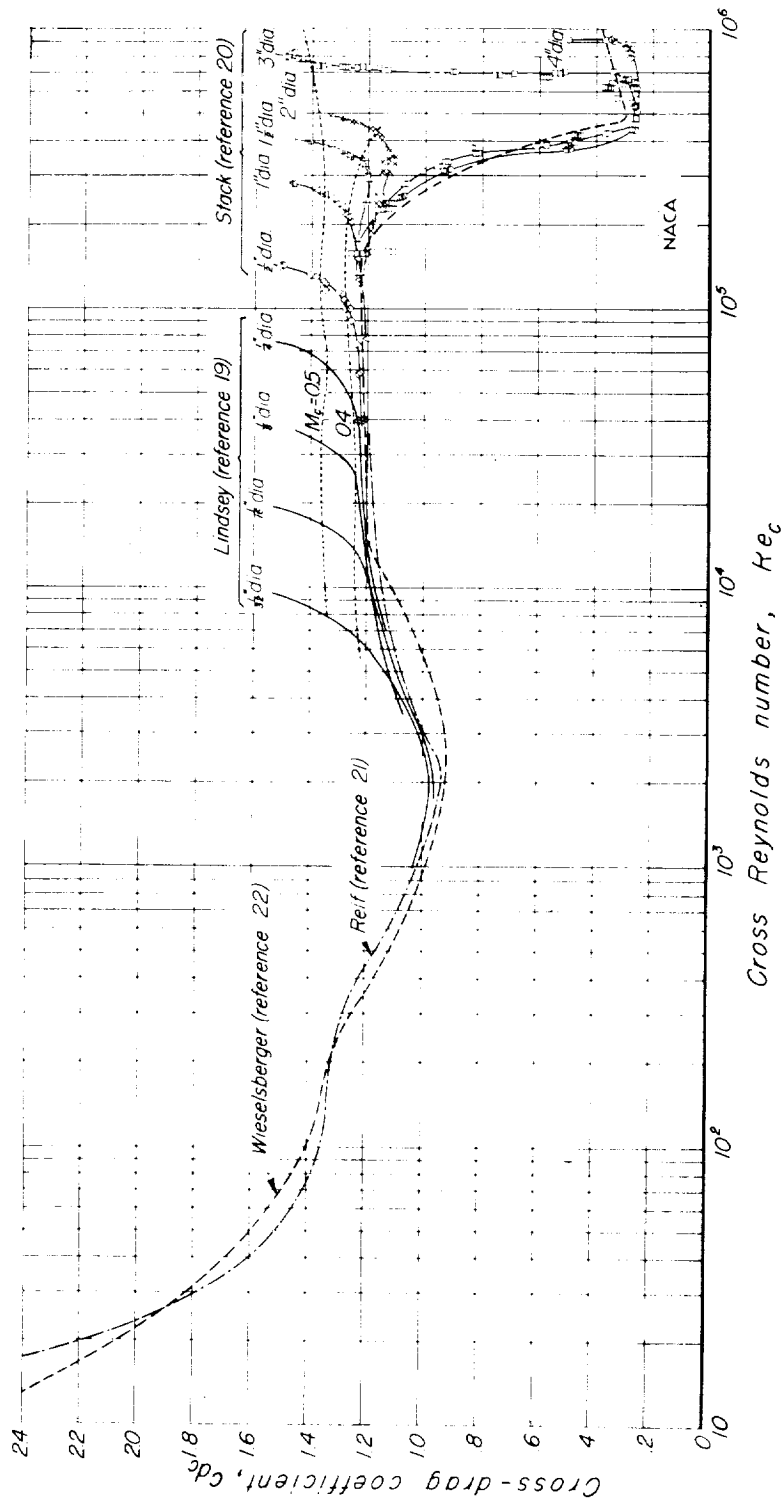


Figure 12.- Circular-cylinder drag coefficient as a function of Reynolds number.

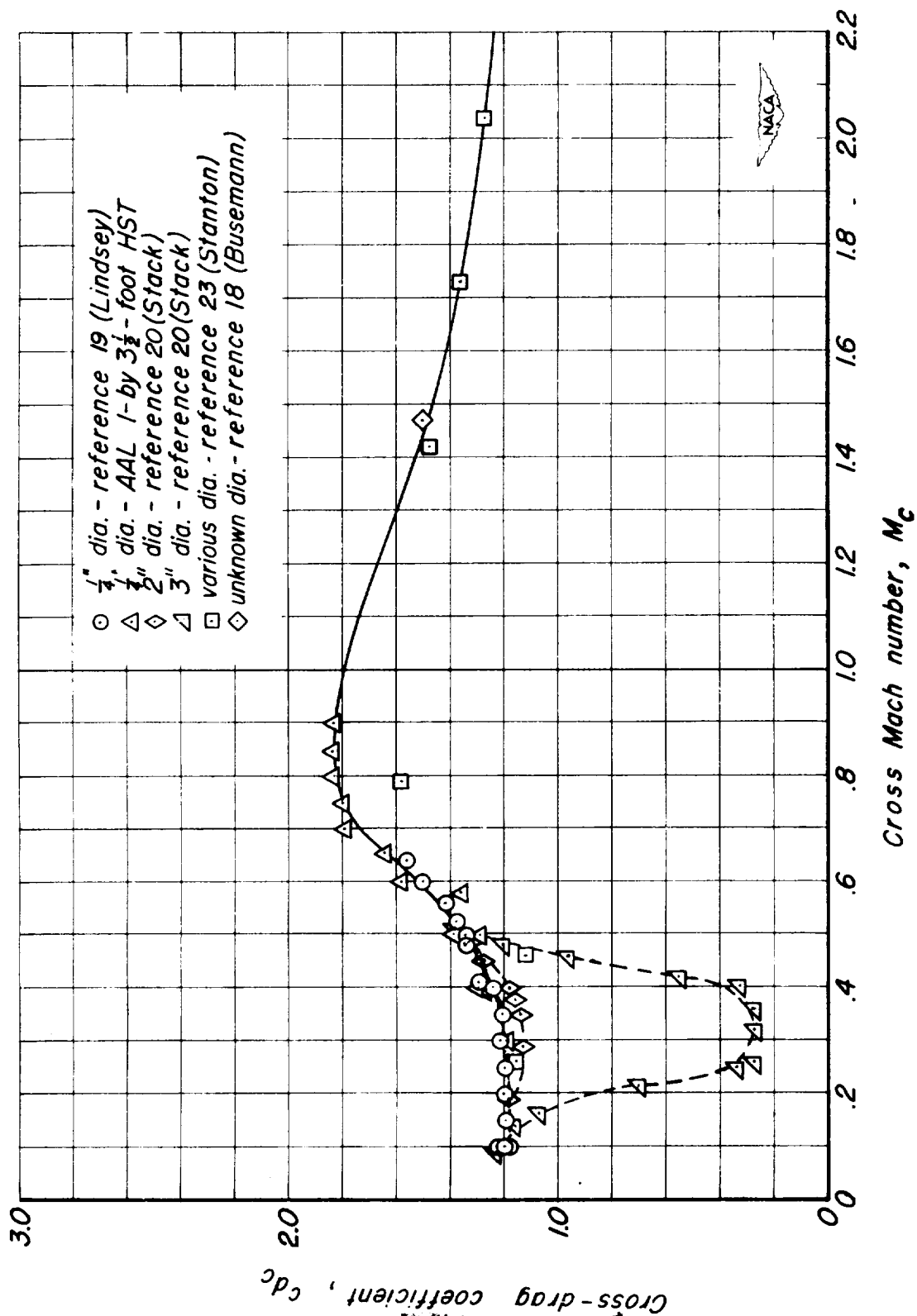


Figure 13. — Drag coefficients of circular cylinders of various sizes as a function of Mach number.

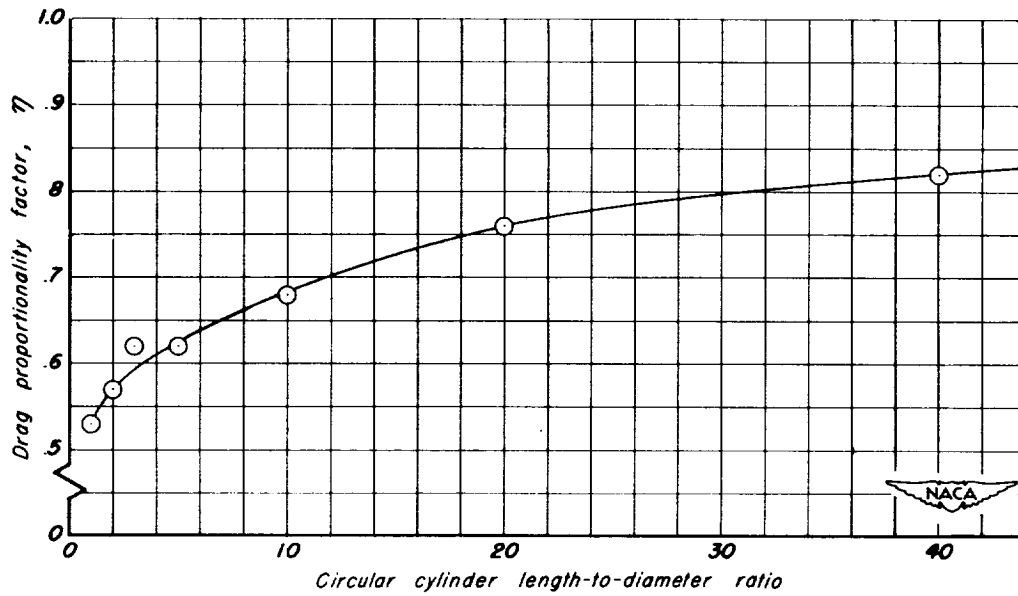


Figure 14.—Ratio of the drag coefficient of a circular cylinder of finite length to that of a cylinder of infinite length, η , as a function of the length-to-diameter ratio. ($R_c = 88,000$).

$$\Delta P = P - P_{a=0} = (2 \tan \beta \cos \theta) \sin 2\alpha + (1 - 4 \sin^2 \theta) \sin^2 \alpha$$

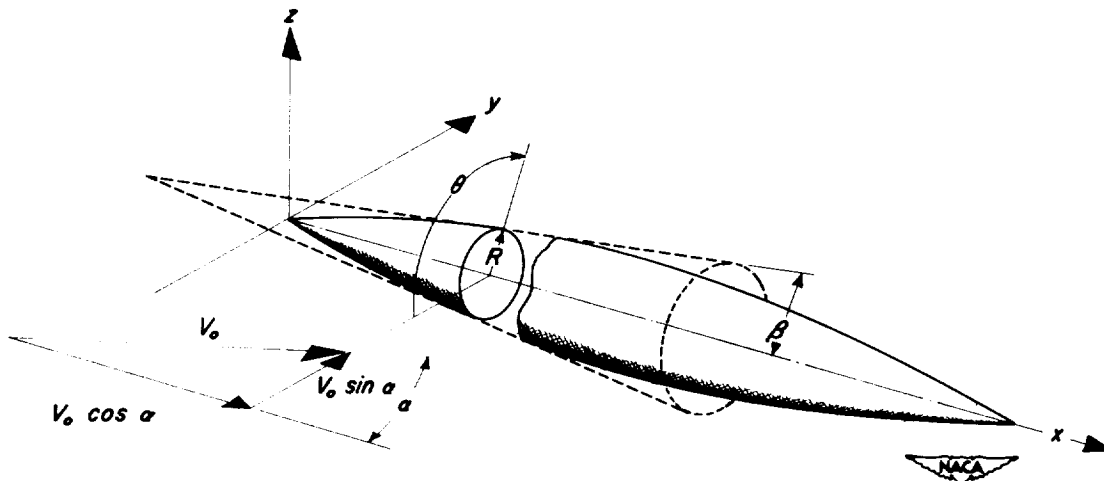
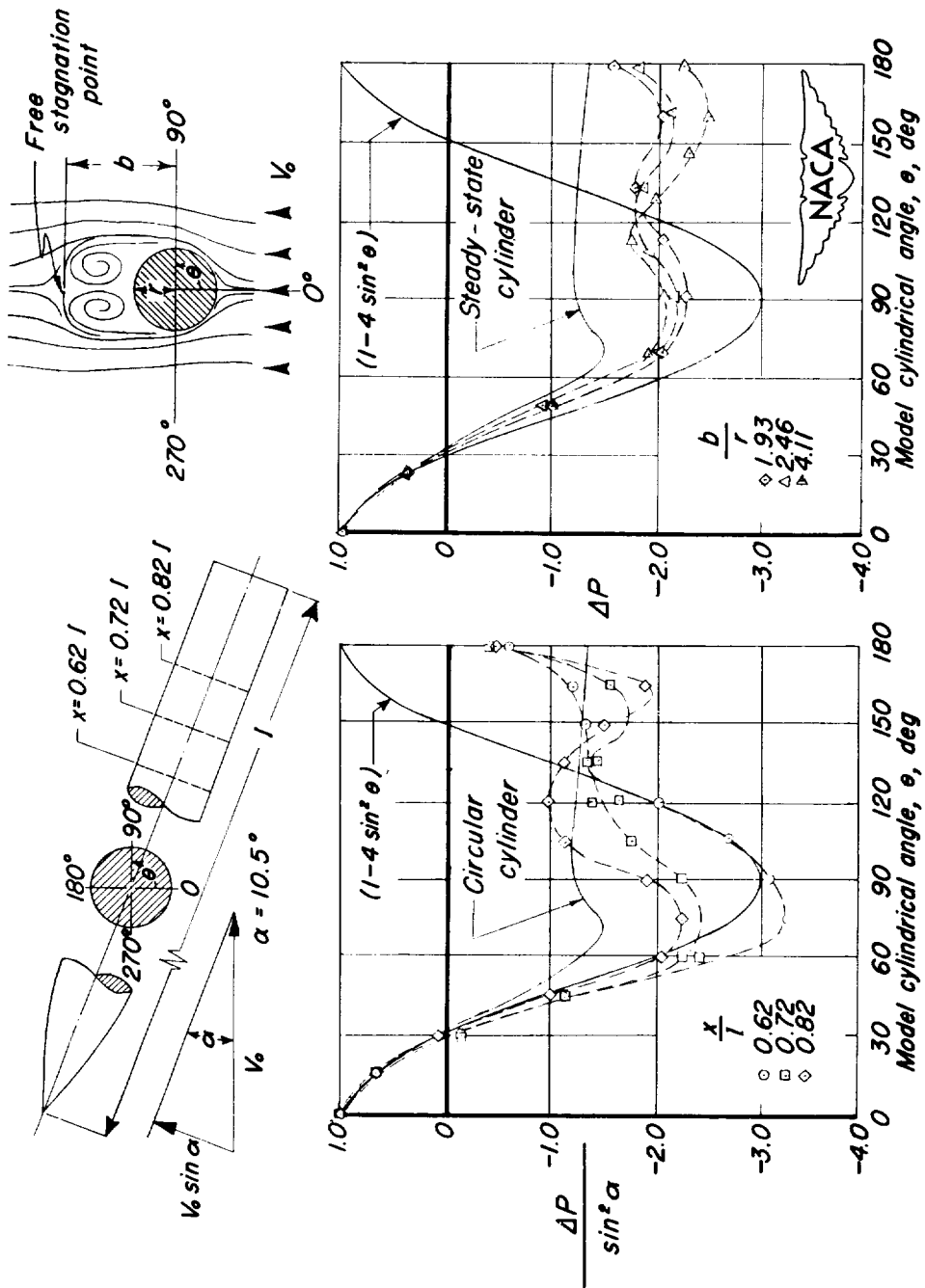


Figure 15.— Incremental pressure distribution due to inclined flow on a body of revolution.



(a) Inclined body and circular cylinder in steady-state motion.

(b) Circular cylinder set in motion impulsively from rest.

Figure 16.- Comparison of the pressure distributions for an inclined body of revolution with that for a circular cylinder.

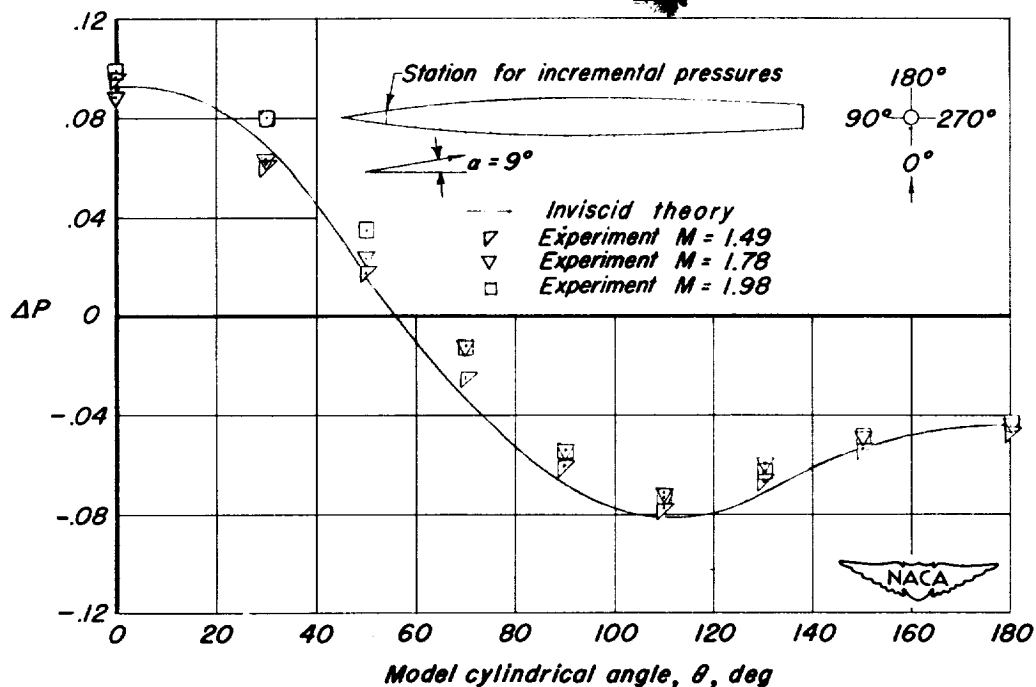


Figure 17.- Incremental pressure coefficient due to an angle of attack of 9° as a function of angular position around the surface of RM-10, $\frac{x}{l} = 0.082$ (reference 26).

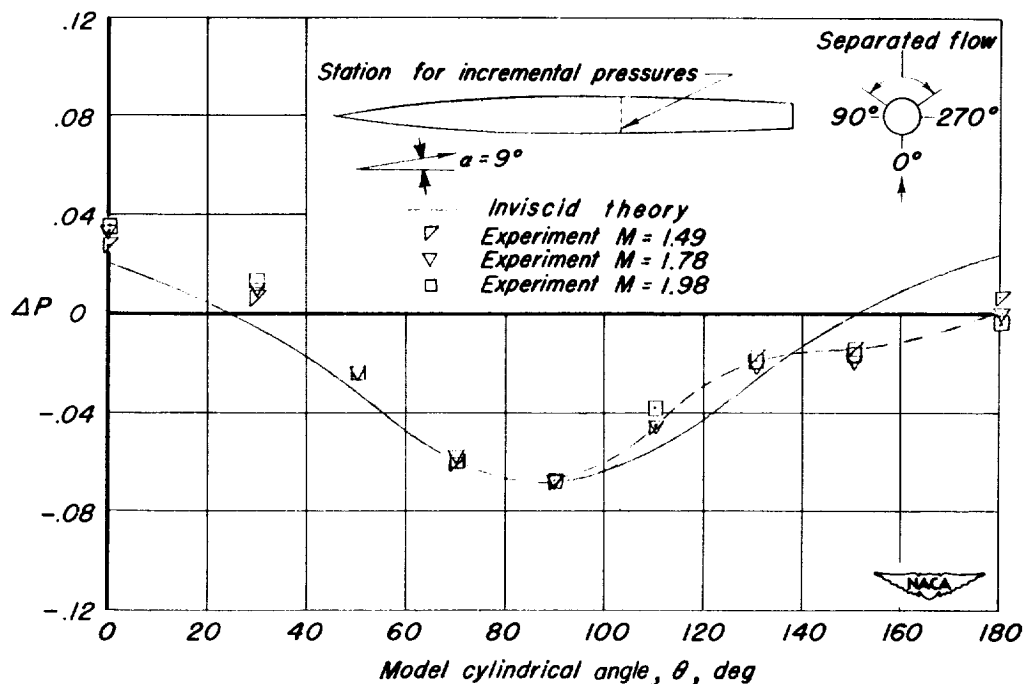


Figure 18.- Incremental pressure coefficient due to an angle of attack of 9° as a function of angular position around the surface of RM-10, $\frac{x}{l} = 0.663$ (reference 26).

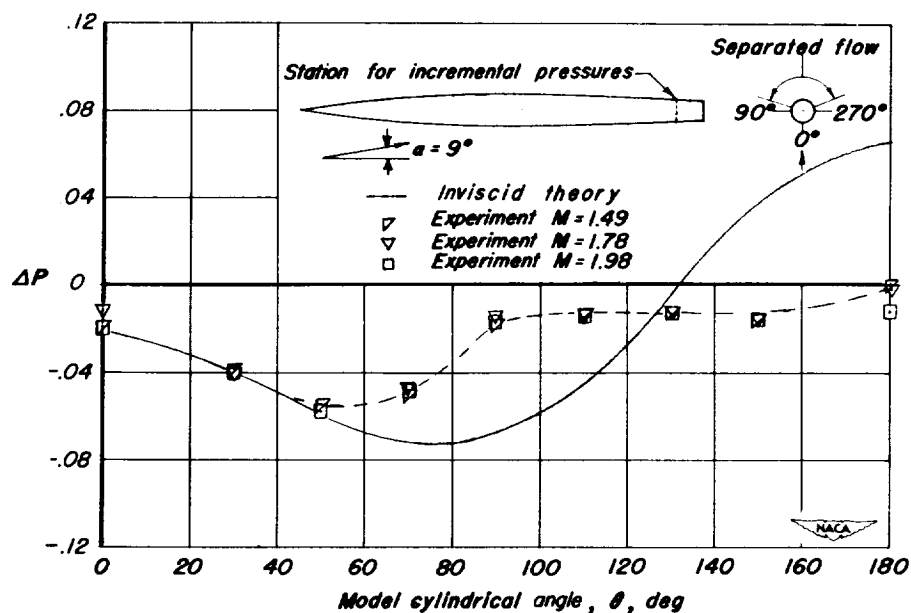


Figure 19.—Incremental pressure coefficient due to an angle of attack of 9° as a function of angular position around the surface of RM-10, $\frac{x}{l} = 0.957$ (reference 26).

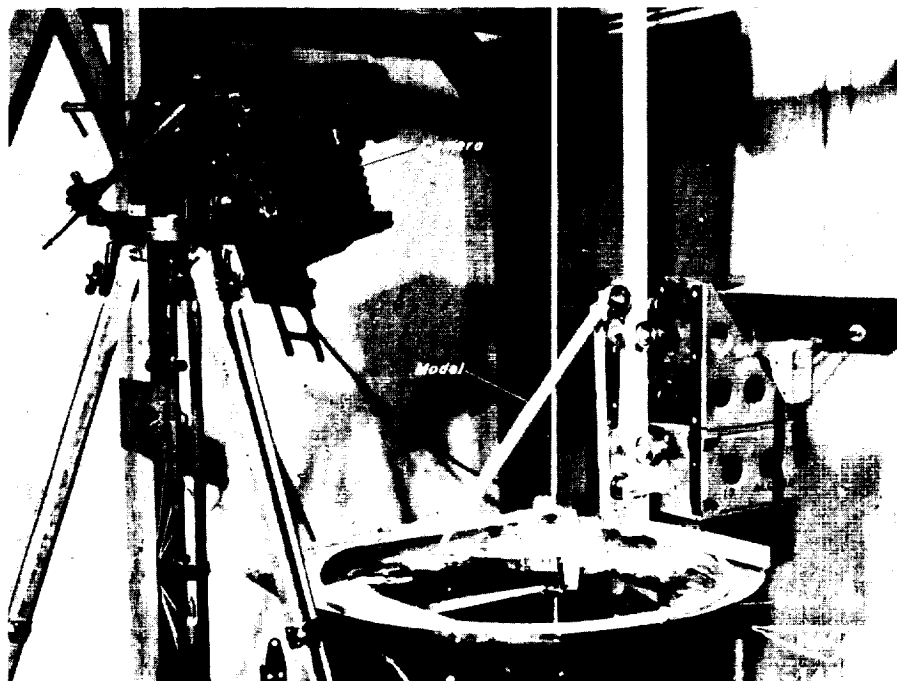


Figure 20.—Apparatus for tests in the water tank with camera and model in place.

1

2

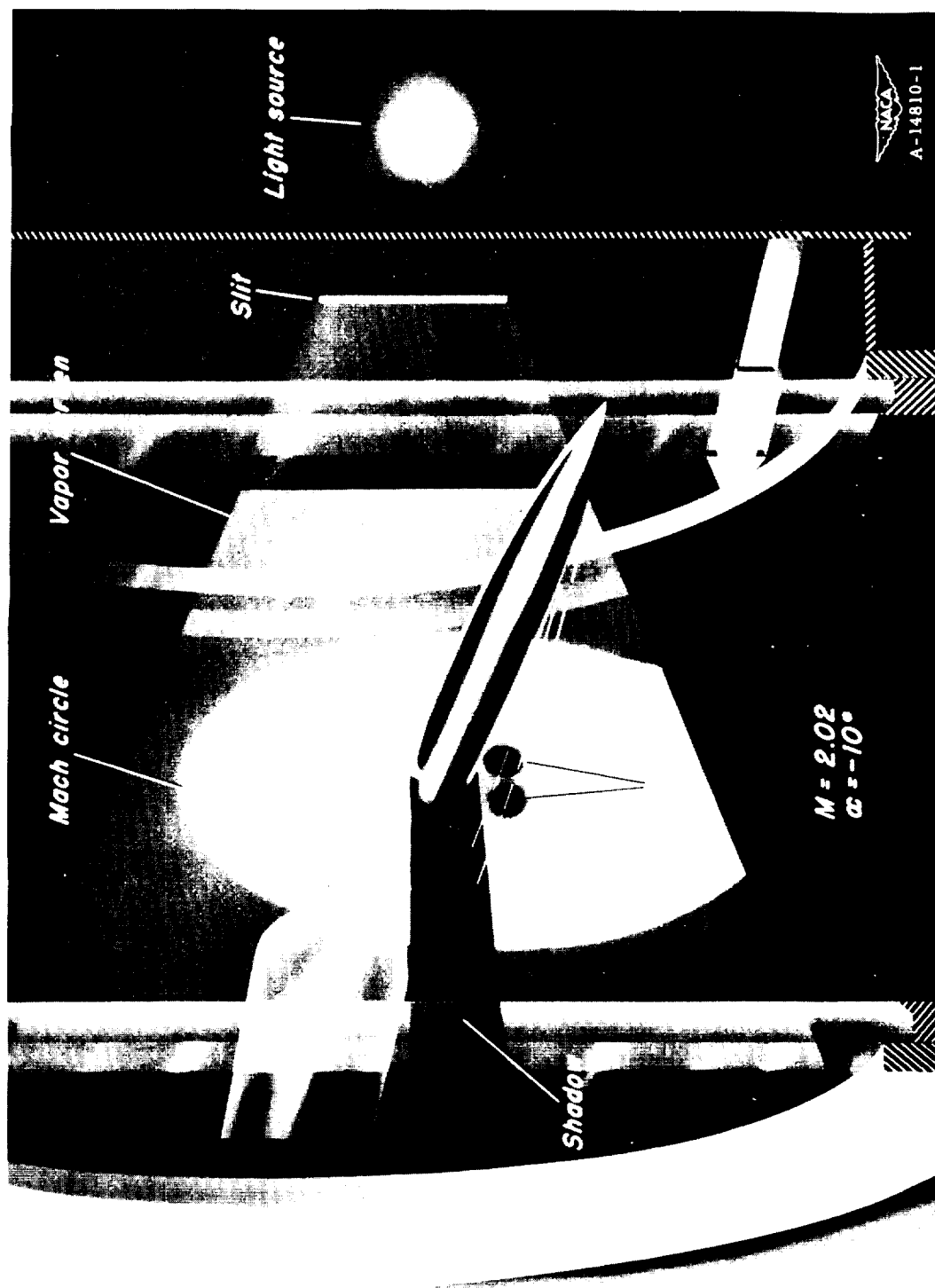


Figure 21.- Schematic diagram of vapor-screen apparatus showing vortices from a lifting body of revolution.



WATER TANK
 $\alpha = 15^\circ$




WIND TUNNEL 
M = 1.98
 $\alpha = 15^\circ$ A-14829-14

Figure 22.— Comparison of the results of the cross-flow studies in the water tank and the wind tunnel.



WATER TANK
 $\alpha = 35^\circ$



WIND TUNNEL 
M = 1.98
 $\alpha = 35^\circ$ A-14829-15

Figure 23.— Comparison of the results of the cross-flow studies in the water tank and the wind tunnel.

